AD-A163 615 ADAPTIVE CONTROL LEARNING AND COST-EFFECTIVE SENSOR SYSTEMS FOR ROBOTICS O..(U) CHARLES STARK DRAPER LAB INC CAMBRIDGE MA J L NEVINS ET AL. 31 DEC 85 1/1

UNCLASSIFIED CSDL-R-1829 N00014-83-K-0587 F/G 6/4 NL

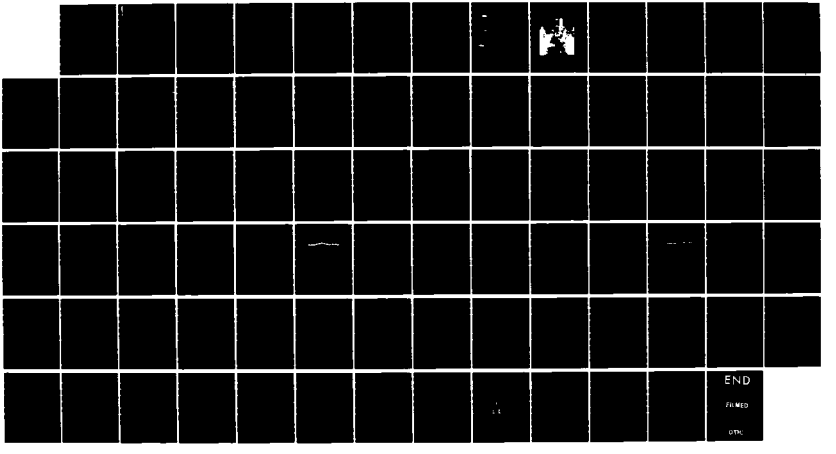

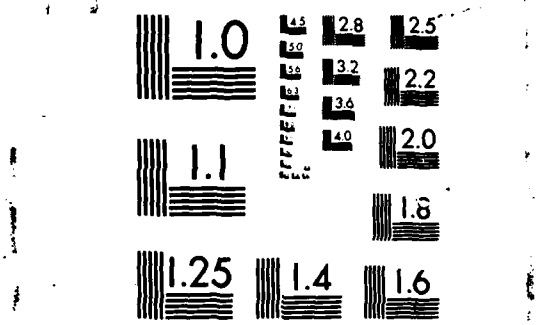

MICROCOPY RESOLUTION TEST CHART
NATIONAL BUREAU OF STANDARDS-1963-A

CSDL-R-1829

ADAPTIVE CONTROL, LEARNING, AND COST-EFFECTIVE SENSOR SYSTEMS FOR ROBOTICS OR ADVANCED AUTOMATION SYSTEMS

by

J. L. Nevins, A. C. Edsall, T. M. Stepien, M. E. Kalinski,
A. A. Karadeniz and R. W. Metzinger

August 1, 1984 – December 31, 1985

The Charles Stark Draper Laboratory, Inc.
Cambridge, Massachusetts 02139

CSDL-R-1829

- Final Report -

ADAPTIVE CONTROL, LEARNING, AND COST-EFFECTIVE SENSOR SYSTEMS FOR ROBOTICS OR ADVANCED AUTOMATION SYSTEMS

Research Focus: Automatic Data Interpretation of Low-Speed Dynamometer Torque Traces Used to Inspect Precision Ball Bearing Assemblies

ONR Contract No. N00014-83-K-0587

J. L. Nevins, A. C. Edsall, T. M. Stepien, M. E. Kaliski,*
A. A. Karadeniz and R. W. Metzinger

August 1, 1984 - December 31, 1985

*Northeastern University
Electrical and Computer Engineering Department

TABLE OF CONTENTS

1.0 INTRODUCTION

1.1 General Discussion

Advanced applications of robotic and automation technology to manufacturing processes and to remote environments such as space and underwater require the performance of complicated but somewhat unspecified tasks. These tasks, usually performed by humans, are unspecified in the sense that they are goal-oriented but without detailed algorithms or methodologies. Furthermore, automated systems capable of performing these tasks must often operate with incomplete or incorrect process models, noisy sensor data, and various constraints.

Tasks for robots can be classified in a number of ways. We tend to define the tasks into two broad classifications - deterministic and non-deterministic. Deterministic tasks tend to be dominated by geometry, part placement, pegs-into-hole, machine load/unload, etc. (Figure 1-1)[1].

Non-deterministic tasks are those done by skilled people involving processes for which models either do not exist or are poorly understood. Other non-deterministic tasks involve inspection or data interpretation and planning[2,3].

The hypothesis of this grant is that the non-deterministic class of problems is amenable to the techniques and methodologies of control system engineering, a discipline which provides a tractable approach for addressing the issues for intelligent systems with cost effectiveness and performance optimality.

The objectives of this grant are:

a. To explore the use of adaptive-learning control systems to complex processes, or engineering-based expert systems to an inspection type task. Both types of tasks, which are usually performed by humans, involve modeling and control or automatic data interpretation in the presence of noisy data with incomplete and time-varying models.

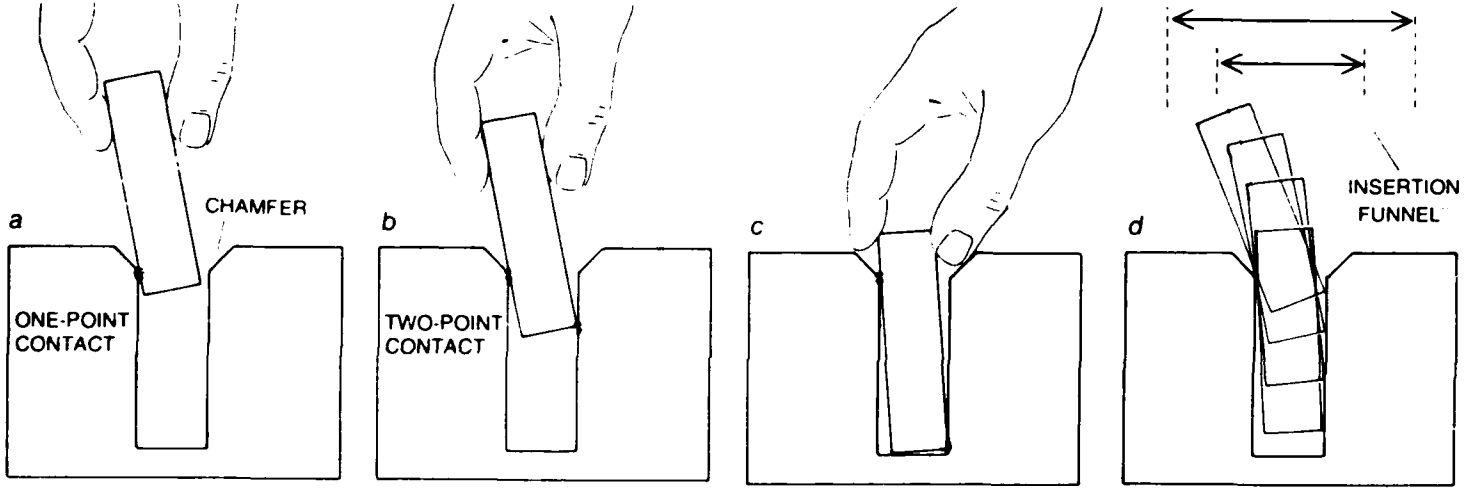

INSERTION OF A PEG IN A HOLE, a typical assembly task, is basically a problem in positioning. Holes are usually chamfered (beveled around the edge) to aid insertion. As the peg slides down the chamfer and enters the hole (*a*) it touches one side of the interior first (one-point contact). If the angular misalignment is large (*b*), the peg will soon touch the opposite side of the hole as well (two-point contact), with danger of jamming. In manual assembly vision can help to find the chamfer, but after the peg enters the hole one must rely on the ability to sense the resisting forces in order to maneuver the peg to the bottom (*c*). The geometry of the peg and the hole keeps the peg within the insertion "funnel" (*d*), the path that is traced by the top of the peg at successively deeper stages of the two-point contact. The smaller the clearance between the peg and the hole, the narrower the insertion funnel and the more difficult the insertion task.

Fig. 1-1. Deterministic Tasks: Insertion of a Peg into a Hole

b. To determine the relevance of these approaches to research on intelligent robotic systems.

c. To determine a focus for testing these theories both analytically and experimentally, if possible.

1.2 Problem Statement

Present-day industrial robots and programmable automation systems[4,5,6] generally perform deterministic tasks. These systems operate with minimal sensing and use a control strategy based on open-loop positioning. That is, the reproducibility of the process is determined by the reproducibility of the machine, the tooling used to hold parts, and the quality of the parts themselves. Sensor requirements for deterministic tasks are modest, mainly monitoring or sequence verification. Examples are presence/absence of parts, task initiation/completion, unexpected hazard and safety. There is a range of sophistication. The classic example is pegs into chamfered holes[1]. Early work suggested 6-axis force sensing and control,[7-10] which is intellectually interesting but a little slow, complicated and expensive. More clever devices[11,12,13] were faster and less complex. The Remote Center Compliance (RCC)[11,12] is even simpler, requires no sensing, has reasonable bandwidth, and is relatively inexpensive (Figure 1-2). More interesting is the problem of pegs into square or non-chamfered holes - "chamferless insertion." At the Draper Lab, the solution has been a kinematic inversion[14,15] (Figure 1-3). It is simple and elegant but seldom used. A more interesting solution is a software kinematic inversion[16] using the Instrumented Remote Center Compliance (IRCC)[16,17]. The IRCC is simply the RCC with added positional sensors for monitoring the displacement of the engineered compliances of the RCC. Since the compliances are known the position sensing can be interpreted as a displacement vector

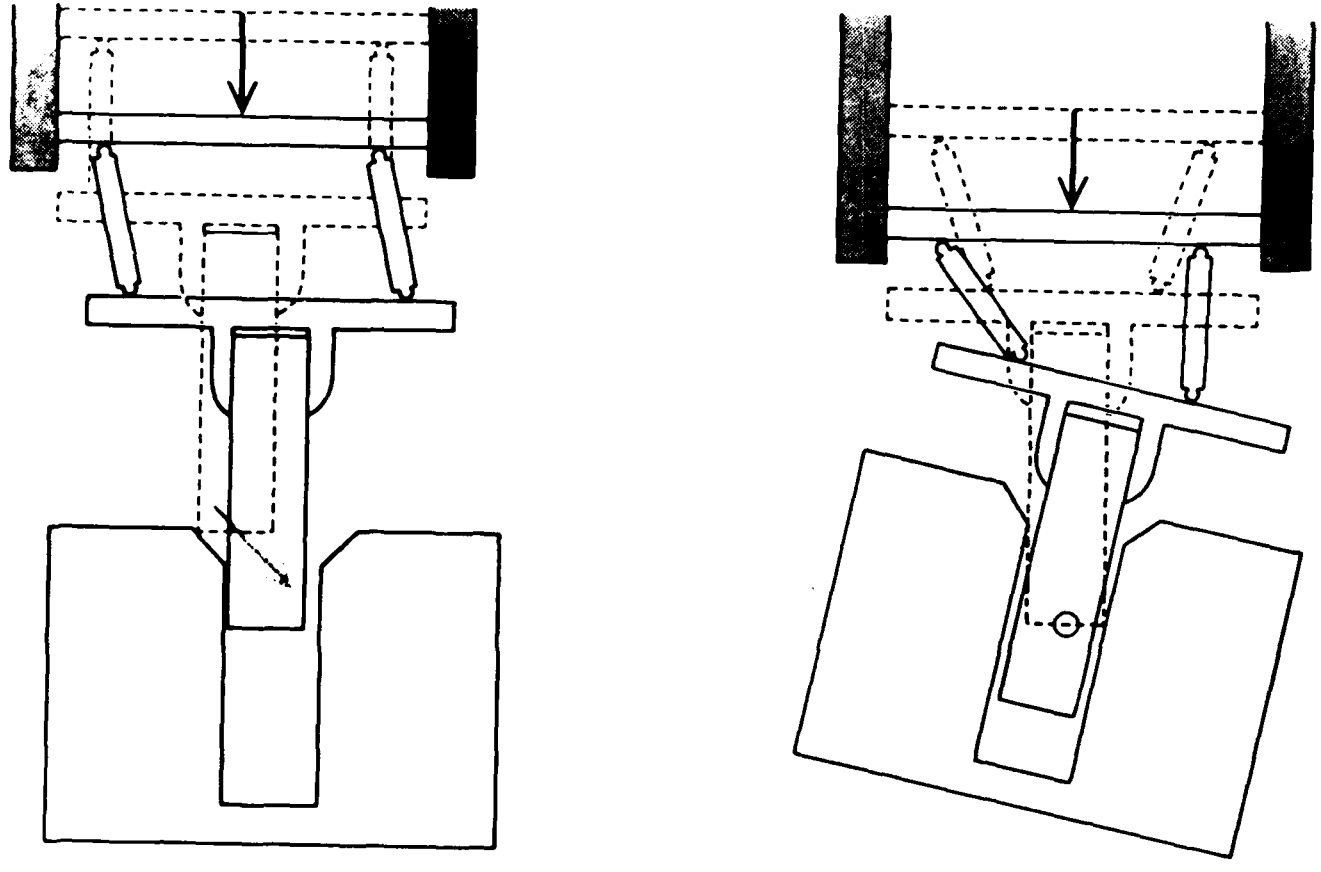

GRIPPERS WITH LINKAGE SUPPORTS can provide the proper response to an error either in lateral position (*left*) or in angular position (*right*) but not in both. The first linkage allows a laterally misaligned peg to slide down a chamfer and enter a hole without rotating. Second linkage allows a misaligned peg to become aligned by rotating at the tip without moving sideways.

Fig. 1-2. The Remote Center Compliance

Fig. 1-3. Kinematic Inversion:
Chamferless Insertion - Mechanical

caused by positioning errors, angular misalignment, small hole or high piece part tolerances or as a force vector resulting from such errors.

Other uses of the IRCC arise from having a "smart finger" on the end of the robot. Automatic teaching, automatic calibration/recalibration, time-position error monitoring are some of the applications[16]. Typical devices have 3 to 6 axes of measurement, so it is possible to monitor either the principal errors or the full error vector including time and environment dependency. Since IRCC's have relatively large position motion compared to 6-axis force sensors[18,19], they are easier to protect from mechanical overloads.

The above listing of tasks and technologies are merely illustrative. Admittedly, there is a slight bias towards using the minimum technology to accomplish the desired task.

Non-deterministic tasks are more interesting and challenging technically. Further, they provide the intellectual base and arguments for intelligent robots. At this point, we really have not attempted to completely classify them. Some classifications are tasks involving process control, monitoring/inspection tasks, and planning tasks. Problems, of course, can be hybrids of these three. Assembly systems usually involve all three. Today the three activities are usually discrete; manufacturing functions are not an integrated activity.

Figures 1-4 and 1-5 illustrate the two types of tasks that have been explored under this grant[20]. Namely, a process task and an inspection task. Automatic planning functions are not part of this grant. However, similar approaches to planning can be found in references (2) and (3).

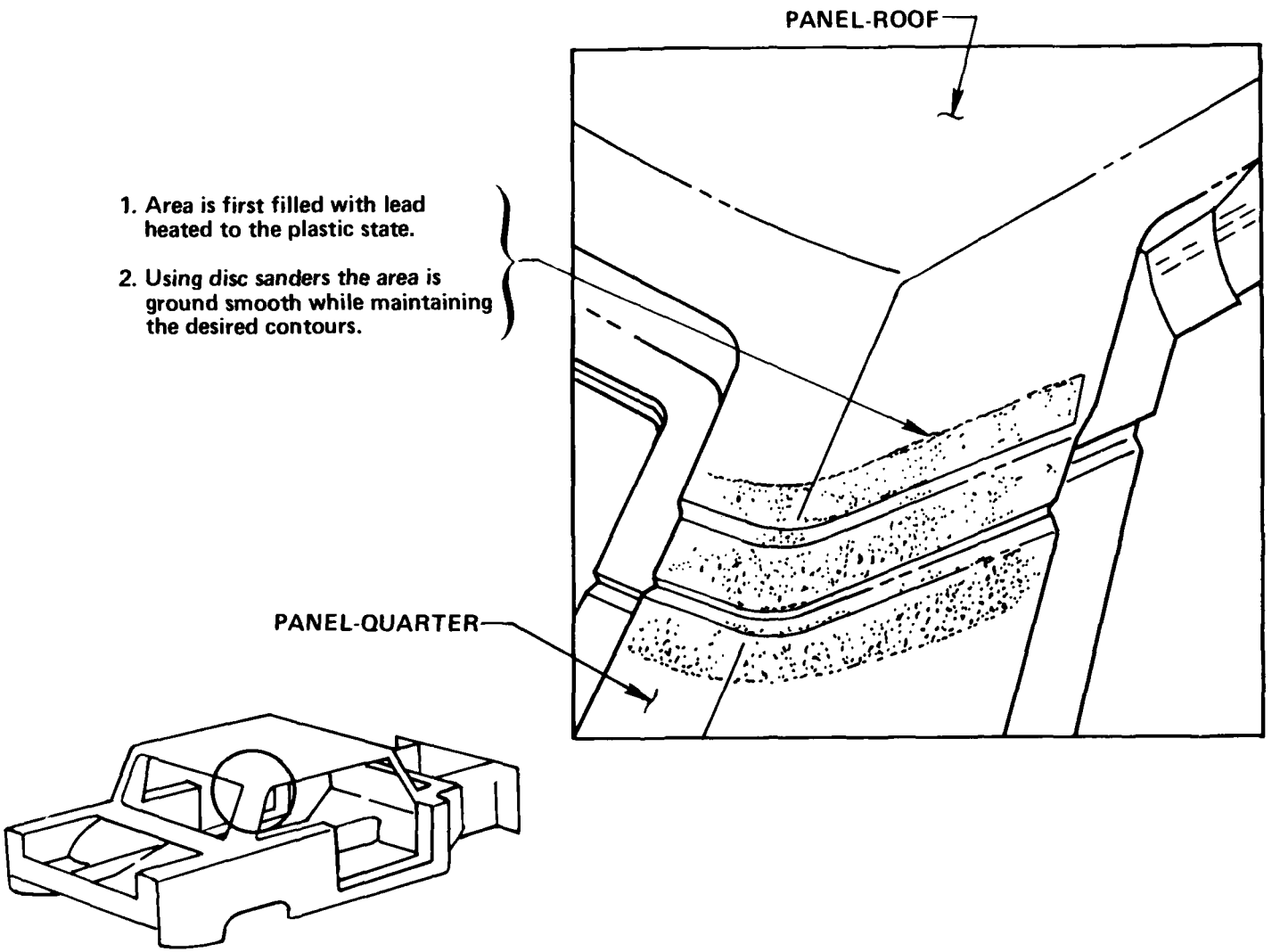

Fig. 1-4. Automotive Body Grinding

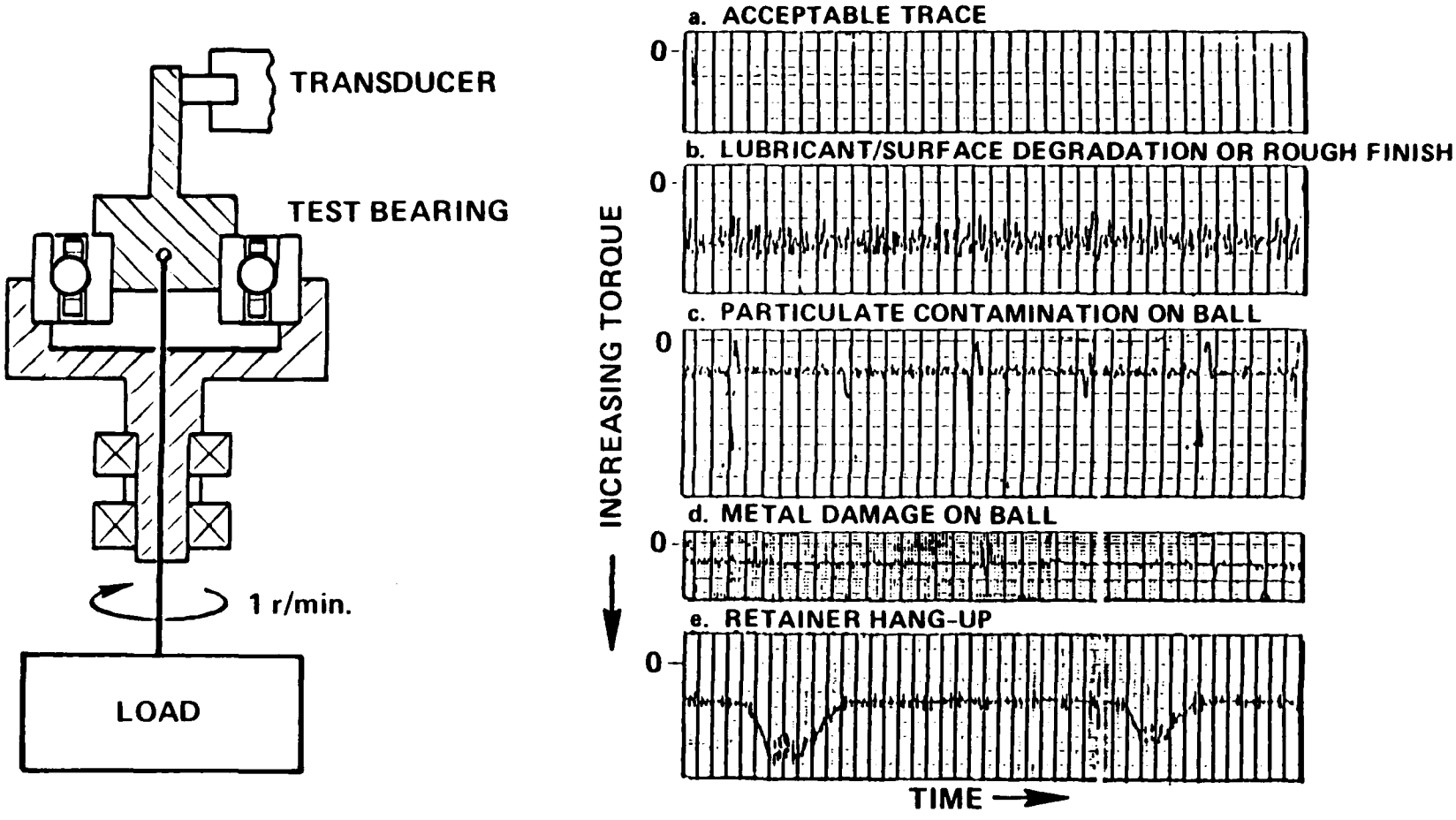

Fig. 1-5. Low-Speed Dynamometer and Typical Torque vs. Time Plots

Figure 1-4 illustrates a manual grinding/finishing task and Figure 1-5[20,21] illustrates the data interpretation task of low-speed dynamometer torque traces for precision ball bearings. Figure 1-4 represents the type of process tasks done by skillful people. Typically these are tasks where complete or partial process models do not exist, performance requirements are not quantifiably stated, and process parameters are time and environment dependent. Yet these tasks are routinely carried out by people. For the task shown in Figure 1-4 (automobile body finishing) the typical process sheet instruction to the operator states "grind it smooth." The trivial question is "What robot system or mechanization can you turn to and tell it to 'grind it smooth'?"

The grinding/finishing task involves three complicated activities and several minor ones. The principal ones are surface reconstruction, process control, and dynamic surface measurement interaction. By surface reconstruction we mean discrete surface measurements and associated algorithms necessary to describe the surface in some convenient computational frame of reference. Minor tasks involve establishing a common computational frame of reference for relating all the process parameters: actual car body location, actual car body shape, and errors in the robot arm.

Weld beads are typically 10-15 mm wide and 2-5 mm high, although much larger and much smaller ones can be found. The bead, in general, lies on a curved surface in space, and the task is to remove the bead and leave the surface the same general shape, with the bead region interpolated in some nonlinear way in the surrounding region.

The data interpretation, or inspection, task shown by Figure 1-5 represents the type of task done by people with judgement developed from many years of experience[22]. The basis for their judgement is generally founded on incomplete understanding of the underlying physics. The problem for the operator is to determine whether the low-speed dynamometer data recorded indicates that the bearing is good or bad and whether it will have

a long or short life expectancy. The operator must determine if the lubricant is sufficient or has degraded (increase in the average noise level), if the bearing contains particles of contamination or has metal damage (specific torque artifacts), if there is misalignment between bearing pairs, or whether the bearing preload is correct.

1.3 Research Focus

The initial problem posed as a research focus was the process problem - manual finish grinding of automobile body filler material used to cover seams between body panels. The prime focus was shifted away from this topic for two reasons. First, it was extremely difficult to develop a reasonable grinding model for testing our theories in the time frame of this grant. The second reason was that since we had two grants in this area (NSF[1] and ONR) a broader research program would result if there were two foci instead of one. That is, one focus on process tasks and the other on inspection tasks.

Before the shift in focus occurred, the problem had been divided into two major research activities: a) geometry or surface reconstruction of a surface from height measurements above a reference plane, and b) process control. One S.M. thesis on surface reconstruction was generated during the time frame(23).

The principal focus of this grant during this past year has been the inspection or data interpretation problem. The test bed for testing theories was the low-speed dynamometer used for testing precision ball bearing assemblies.

Inspection tasks are important because automating groups of tasks usually requires multi-level inspection to be performed. Levels vary from simple binary go/no-go decisions, which are

---

[1] NSF Grant No. ECS-8214366, reference (22)

easily automated, to more complex questions which cannot be answered readily. Decisions on higher inspection levels often must be made by experienced experts or well-trained consultants.

One test used to inspect precision ball bearings prior to, during and after their assembly is the low-speed dynamometer (LSD) test. The low speed dynamometer(24), shown in Figure 1-5, measures the drag torque between the bearing races while the bearing is rotated at a slow speed. Manual inspection of these analog traces can reveal significant information on the quality of the bearing including the presence/absence of dirt particles, metal damage to balls or races, lubrication degradation and bearing retainer hang-up. Individual torque traces, as well as an ensemble of traces over time, are important in determining the acceptability of the bearing.

The hypothesis that we used is that this class of problems is amenable to the techniques of control system engineering and artificial intelligence - particularly a new technique called the engineering-based expert system.[2] The engineering-based expert system captures, algorithmically, the capabilities of human "experts" and trained process operators in an efficient and cost-effective manner. It combines techniques of process modeling and identification, signal processing and detection, pattern recognition, hypothesis testing, control theory, as well as the conventional expert system's rules and heuristics.

The general objective of this research was to apply engineering-based expert system techniques to complex manufacturing tasks which traditionally require the expert or artisan skill of a human.

---

[2] The concept was new when this grant proposal was written several years ago. Since that time a number of people have become interested in this approach.

1.4 Report Organization

The research carried out has demonstrated the feasibiity of an engineering-based expert system for the inspection task chosen. Further, a Navy program office has decided to implement the technique into a production environment in one of their suppliers of precision mechanisms.

The remainder of this report is organized as follows:

Section 2.0 Research approach.

Section 3.0 Research, prototype system, and comparison with the manual method.

Section 4.0 Conclusions, and recommendations for further research.

2.0 RESEARCH APPROACH

2.1 Traditional Expert Systems

Artificial intelligence (AI) may be loosely defined as the science of enabling machines (computers) to learn, reason, and make decisions. The expert system is an AI system which performs a specific function normally performed by a human expert. The term expert implies that a substantial amount of acquired skill and knowledge is required to perform the function. The AI expert system must embody the required knowledge and have an algorithmic structure by which to process external inputs in the context of this knowledge. In the traditional expert system, the knowledge exists in the form of heuristic rules. These rules are heuristic because they are derived from experience rather than fundamental scientific principles. Physical models based on first principles are seldom explicit in the knowledge base but may be implicit in the rules specified by the expert. In this way, the traditional expert system is imitative; it attempts to duplicate the human's reasoning process without attention to the underlying science of the problem at hand. An overview of traditional knowledge representation methods may be found in reference(25).

The algorithmic structure by which the rules are implemented can be one of several types(26). The forward-chaining or data-driven structure proceeds from the available data and invokes rules as required to find a path to a goal or conclusion. In the backward-chaining or goal-driven structure, a goal is specified by the hypothesis of a conclusion. Rules are then invoked and data is acquired to verify all necessary antecedent conditions or subgoals. Thus a path from the data to the conclusion is found in reverse. In general, the nature of the problem dictates which structure is more favorable. It is possible to combine forward-chaining a d backward-chaining.

The traditional expert system concept has been applied to the fields of medical diagnosis, machinery troubleshooting,

geophysical exploration, engineering design, and many others[26]. A very brief summary of a few successful systems is presented here.

In medical diagnosis, expert systems are used to deduce medical conditions given a set of observed symptoms. Perhaps the best known system is MYCIN[27]. MYCIN was developed in the 1970's at Stanford University to aid physicians in the selection of antibiotics for the treatment of severe infections. The system contains about 500 rules associated with medical diagnosis which are implemented in a goal-driven architecture. MYCIN incorporates the capability for the user to inquire why and how conclusions were reached. Although generally considered an academic success, MYCIN has not been accepted in the health care industry. MYCIN is not used to detect symptoms, only to analyze them according to heuristic rules defined by an expert. Another medical diagnosis system, PUFF[28], incorporates the ability to automatically acquire data on a patient's pulmonary functions. This data and background information supplied by a physician are interpreted according to a set of 55 "if-then" rules to diagnose pulmonary function disorders. Much work has been done in the automatic interpretation of electrocardiograms using statistical pattern recognition methods[29]. However, these systems are generally not considered expert systems because of their basis in pattern recognition and signal processing rather than heuristic knowledge.

Expert systems have been developed for the diagnosis of machinery. One such system, CATS-1[30] is being used to troubleshoot diesel electric locomotives. CATS-1 uses approximately 530 rules in a forward and backward chaining logic to interactively diagnose locomotive problems and suggest repair procedures. Like MYCIN, this is a consultation system and includes no means of acquiring data except through a human operator.

In geophysical exploration, expert systems can be used to identify geophysical structure and features (e.g. oil or mineral deposits) from seismic measurements. One such system, PROSPECTOR,

has located a previously unknown molybdenum deposit[26]. Like MYCIN, PROSPECTOR has no understanding of the basic physical principles underlying its conclusions but is based on a large (but still incomplete) set of heuristic rules.

Expert systems for design have been developed for a number of applications such as the design of V-belt drive trains (VEXPERT)[31], complex gear train design (IMP)[32], configuration of computer components (R1)[26], and heat exchanger design (HEATEX)[33]. Some systems, such as VEXPERT, attempt to embody the methodology of design in rules. VEXPERT uses a Design-Evaluate-Redesign architecture which is applicable to a variety of problems by substitution of the appropriate analysis algorithms and constraints. Other programs such as HEATEX, which uses 115 rules and formulas to design optimal heat exchangers, and IMP stress the analysis inherent in design rather than the methodology. The analytical formulas and design "rules of thumb" associated with a particular problem indirectly represent physical models. The application of these formulas and rules is, however, largely heuristic. R1 is a data-driven system used to determine the physical layout and interconnection of components of computers based on rules of thumb. R1 is in routine use.

All of these systems are based on emulation of the human expert. Logic is rule-based, where the rules are those which the human has chosen to use. Where explicit analysis is required, as in some design systems, the algorithms selected are those which the human can best understand. We argue that these rules and algorithms, which are apparently well-suited to the human mind, are not necessarily well-suited to a digital computer.

2.2 Engineering-Based Expert Systems

The traditional expert system is a problem solving technique which is well suited to problems which cannot be rigorously analyzed for lack of understanding or due to inadequate analysis techniques. For example, medical science is not fully understood

and the use of heuristic knowledge obtained from experienced physicians is necessary in creating systems for diagnosis and treatment. However, if the underlying physics and mathematics of the problem are sufficiently well understood, then the use of heuristic knowledge may not be appropriate. Wherever possible, mathematics is the preferred representation of knowledge for precision, clarity, and the ability to be verified. Figure 2-1 illustrates the typical spectrum of problems and problem solving techniques. Problems range from clear, well understood, fully analyzable to fuzzy, poorly understood, and not analyzable. The applicable classes of systems range from engineering analysis systems to traditional expert systems. The middle ground contains problems which are partially analyzable but also require some degree of human expertise. This class of problems is the domain of the engineering-based expert system. Admittedly, the boundaries between these classes is a matter of arbitrary semantics. However, the salient feature of the engineering-based expert system is the integration of rigorous analytical techniques with heuristic techniques.

The engineering-based expert system is the result of a combination of formal engineering analysis, mathematical processing techniques, and traditional expert system techniques. Analysis leads to a fundamental understanding of the problem and the development of models which can be augmented by the heuristic rules of the expert. The models represent precise knowledge about the problem and the heuristic rules capture the skills of the expert. Mathematical processing can be substituted for human perception and reasoning processes which cannot be adequately expressed as rules. Mathematical techniques may also be used to enhance data prior to the application of heuristic rules by filtering or transforming to a more convenient form. Determining the boundary of analyzability and the optimal combination of heuristics and analysis for particular problems is a future research issue.

Analytical models and heuristic knowledge have been integrated for expert systems in renal physiology[34], for

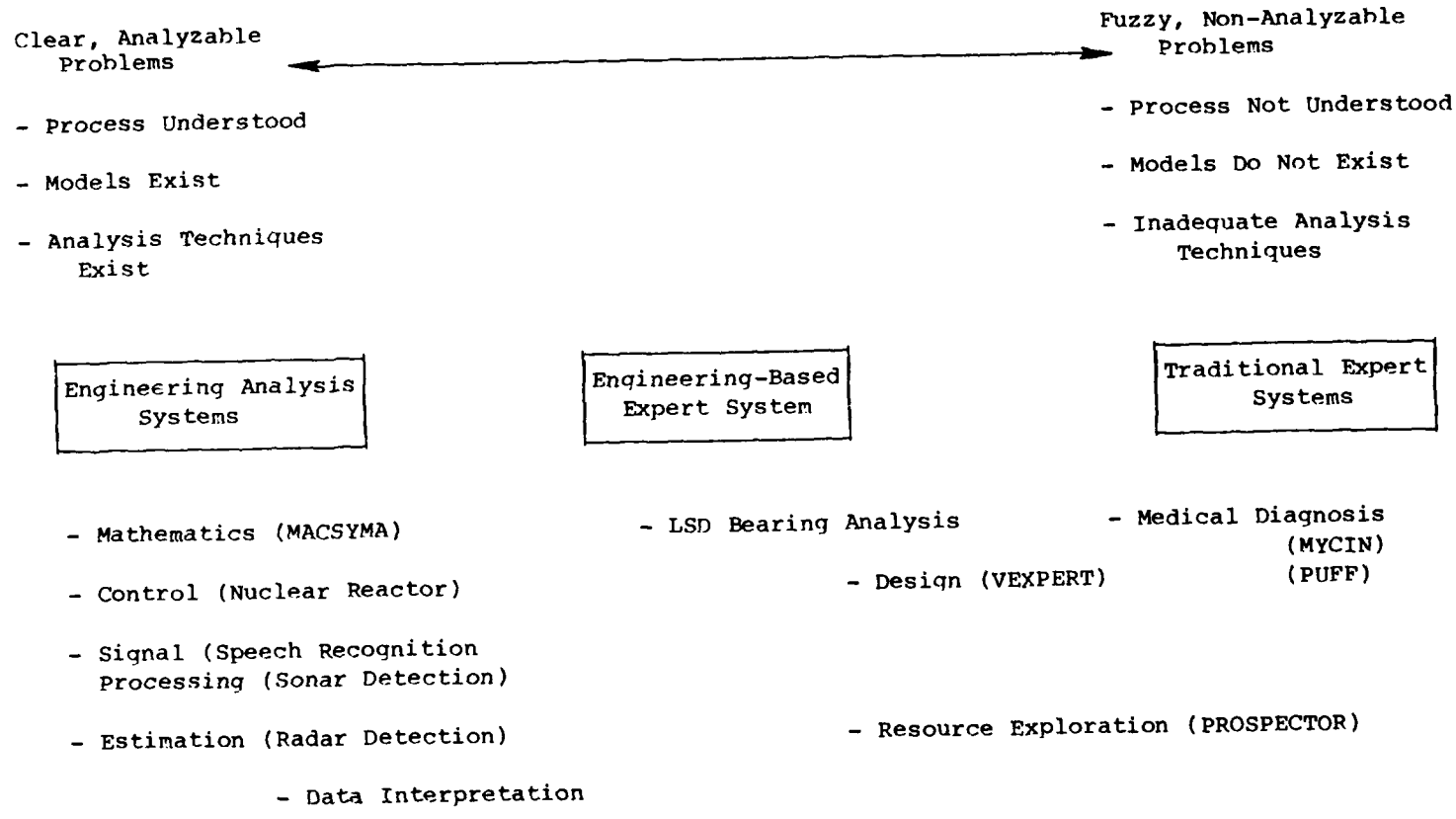

Fig. 2-1. Range of Problems & Problem Solving Methods

process control[35], for control of a nuclear reactor[36], and for intelligent automatic control systems[37] in general.

Mathematical processing techniques from the fields of estimation and control, signal processing, and statistical pattern recognition have been applied to a variety of expert problems such as radar and sonar detection[38,39], electrocardiogram classification[29,40], speech recognition [38], and geophysical testing[38]. These signal processing and pattern recognition systems are not usually considered expert systems because they do not mimic human actions. However, these analytical methods are an important part of the engineering-based expert system concept.

The advantages of the engineering-based expert system approach are numerous:

1. Because of the engineering analysis, rules may be stated in terms of any physical parameters of the problem rather than those solely perceived by the human. Furthermore, redundant or conflicting heuristic rules can be systematically eliminated.

2. The system will be more adaptable to changes in the problem or the environment because many parameters will have a known physical significance. Those changes will be accommodated by parametric variations rather than through structural changes to the system.

3. Efficient mathematical processing can be substituted for less efficient and possibly unpredictable symbolic processing.

4. The engineering analysis will allow rules to be stated in a more concise form and mathematical processing will be the preferred knowledge representation. Therefore, the total number of rules may be reduced.

These advantages are exemplified by the LSD analysis system described in reference (21) and in section 3 of this report.

2.2.1 Knowledge Requirements

The knowledge base for the traditional expert system consists of rules specified by the human expert. These rules are usually stated in a symbolic rather than mathematical form.

The knowledge base for the engineering-based expert system consists of both process models and rules. The process models are the result of formal analysis and represent, in a concise mathematical form, knowledge about the process of interest. The models may express an exact deterministic relationship between the process parameters, inputs, and outputs, or they may express a probabilistic relationship between the parameters, inputs, and outputs (a stochastic model). The rules associated with the engineering-based expert system may be different and fewer in number than the heuristic rules associated with the traditional expert system.

This knowledge base can be more extensive than that of the traditional expert system because the process models may contain information that is not explicitly known by the expert or information that is only implicit in the expert's heuristic methods. In many cases, the experts do not understand the underlying mathematics and physics.

Table I summarizes the distinction between the knowledge bases of the two systems.

Table I: Knowledge Bases

Traditional Expert System	Engineering-Based Expert System
Rules derived empirically from expert	Rules derived from rigorous analysis of process
Little or no physical insight into process	Physical insight through process models
Indirect access to process variables	Explicit access to process variables

2.2.2 Algorithmic Requirements

The primary tool used by the traditional expert system is symbolic logic. Data are processed by making a series of decisions according to the rules specified in the knowledge base.

The engineering-based expert system operates using

- Signal processing and estimation
- Pattern recognition
- Hypothesis testing
- Process models

as well as symbolic processing. The intensive use of numerical computation differs from the traditional expert system approach which relies almost totally on symbolic processing. In general, algorithms may be implemented in a data-driven architecture or a goal-driven architecture. Most signal processing techniques are inherently data-driven, while hypothesis testing can be goal directed.

The distinction between symbolic processing and numerical processing necessitates different hardware and software configurations for the two approaches. Most current symbolic processing languages have inadequate numerical manipulation capabilities. Likewise, conventional numerical processors and languages frequently have inadequate symbolic processing capabilities. The engineering-based expert system requires both capabilities and therefore has unique architectural and language requirements.

3.0 THE LOW-SPEED DYNAMOMETER INTERPRETATION SYSTEM

3.1 Introduction to the LSD Research Problem

An important issue in manufacturing is part inspection and quality control. Inspection operations may provide information about the condition of individual parts as well as information about the status of the manufacturing system. The complexity of inspection operations may vary from simple binary tests, such as the presence or absence of a component, to tests involving extensive measurement and evaluation procedures. The simple operations might easily be automated because only binary yes/no decisions are required. The more complex operations often require trained experts to interpret results and make decisions. These complex decision processes can be automated by embedding the experience and knowledge of the expert in a computer program.

An example of a complex inspection operation is the low-speed dynamometer (LSD) used to test instrument quality ball bearings during their manufacture, assembly, and integration into components[24,41]. The LSD, illustrated in Figure 1-5, measures the torque required to rotate a bearing or bearing assembly at a slow speed - typically 1 revolution per minute. At this slow speed the lubricant film is thin enough to allow virtual metal-to-metal contact between balls and races. Two major mechanisms contribute to this low-speed drag torque: sliding friction forces due to pivoting and slipping motions in the ball-to-race contact zones and geometric profile forces due to asperities of the ball and race surfaces. In lightly loaded instrument quality bearings, the geometric profile torque can be as large or larger than the friction torque. The torques can be distinguished by operating the LSD in two directions - friction torques will reverse polarity with reversed direction while geometric profile torques will not. The torque is usually measured and recorded for 1 or 2 revolutions of the bearing.

Measured torques from both mechanisms can reveal significant information about the condition of the bearing. The sliding

friction torque is indicative of the loading of the bearing and allows the LSD to be used to adjust bearing preload and to identify misalignment of paired bearings. Geometric profile torque can indicate ball or race surface roughness, damaged balls or races, and particulate contamination. The characteristics of the data can be used to determine the exact nature of the geometric profile.

Traditionally, the LSD measurements are interpreted by a trained expert who visually inspects analog plots of bearing drag torque. Although there are deterministic physical relationships between the condition of the bearing and the torque measurement, the expert's methods are essentially empirical. He relies chiefly on visual recognition and experience to assess the quality of the bearing.

This problem falls into the "middle ground" of Figure 2-1 where the physics can be explained intuitively but are not fully analyzable. Therefore, the engineering-based expert system is the appropriate technique for automation. The remainder of this chapter will describe the system that was carried out. Section 3.2 describes typical bearing problems that are revealed using the LSD. Development of detection algorithms and acceptability criteria for bearing artifacts is delineated in Section 3.3. The algorithms and criteria were developed and implemented a computer system which performs LSD interpretation at the level of an expert. The performance of this system is characterized in Section 3.4

3.2 Characteristics of LSD Torque Measurements

Typical time plots of LSD torque measurements are shown in Figure 3-1. Figure 3-1(a) shows a measurement of the low-speed drag torque for 2 revolutions of a bearing of acceptable quality. Figures 3-1(b) - 3-1(e) show torque measurements for several unacceptable bearings.

Figure 3-1(b) shows a torque measurement exhibiting metal damage. The metal damage is characterized by sharp excursions in torque which moves first in the direction of decreasing magnitude

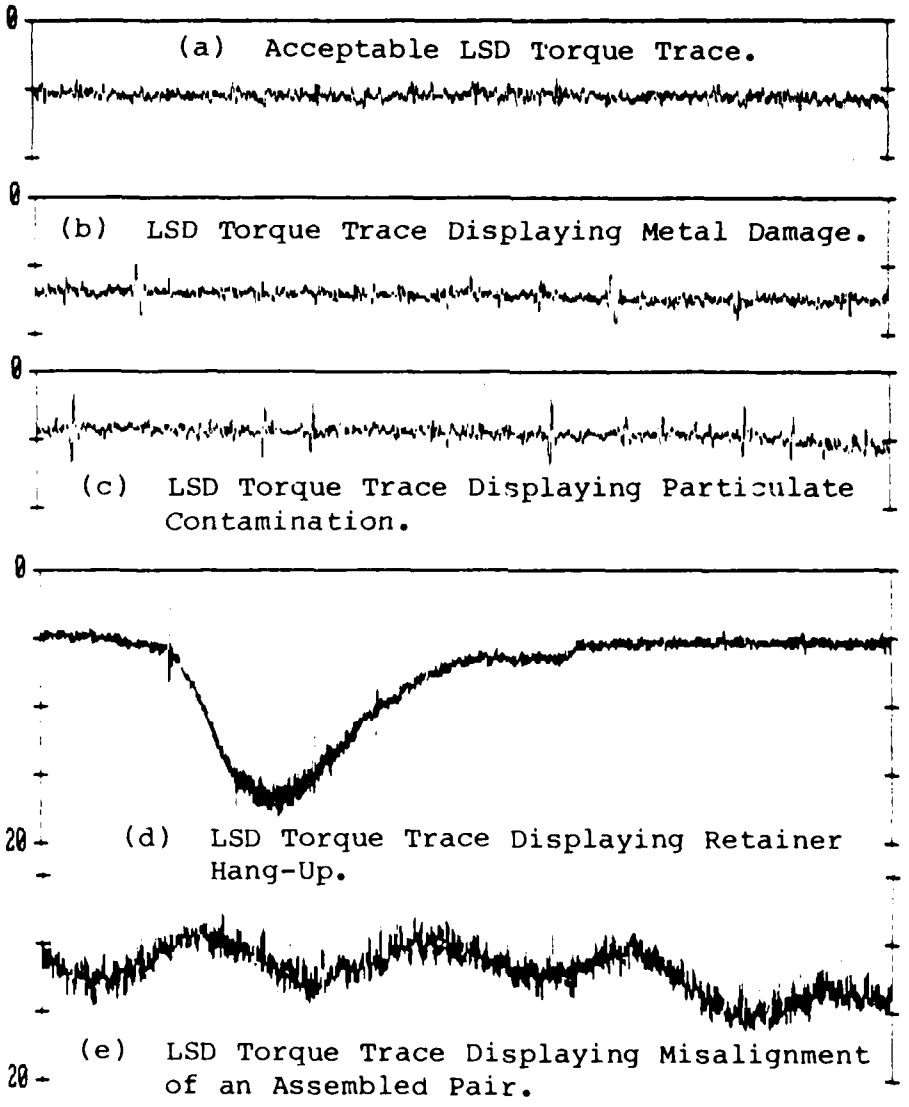

Fig. 3-1. Typical LSD Torque vs. Time Plots

as the ball (or race) rolls into the area of damaged metal followed by increasing torque as the ball (or race) rolls out of the damaged area.

Figure 3-1(c) shows a torque measurement exhibiting particulate contamination. The contamination is characterized by sharp excursions in the torque which move first in the direction of increased magnitude as the ball (or race) rolls onto the particle followed by decreased magnitude as the ball (or race) rolls of the particle.

Figure 3-1(d) shows a torque measurement displaying retainer hang-up. This is evidenced by a slow torque excursion due to increased friction from excessive rubbing of the retainer on balls or races.

Figure 3-1(e) shows a torque measurement displaying misalignment of a preloaded bearing pair. Misalignment results in a sinusoidal torque variation at the bearing rotation frequency.

The distinction of well-developed features associated with different flaws is generally reliable and the expert has no problem identifying and classifying flaws on the basis of these patterns. The expert must identify the bearing problem rather than make a simple good/bad decision because certain problems can be easily resolved whereas others may be irreparable. For instance, contamination can be resolved with a thorough cleaning, but metal damage requires replacement of the race or ball.

If the bearing defect artifacts were as sharply defined as illustrated in Figure 3-1, this problem would be straightforward to solve and not a suitable candidate for research. The artifacts are not, however, distinct. A single torque trace may exhibit more than one defect. There is no guarantee that different bearing failure modes are mutually exclusive. For example, a bearing may suffer from particle contamination, metal damage, and retainer hang-up at the same time. It is important to detect all of these failure modes because each requires a different action on the part of the assembler. In addition, the salient characteristics of the artifacts associated with each failure mode are sufficiently different that no single pattern recognition or signal processing technique is likely to be effective for all

modes. The development of the various detection algorithms and acceptability criteria is described in the next section.

3.3 Development of the LSD Interpretation System

3.3.1 Interpretation Rules

The LSD expert evaluates the quality of bearings by visually inspecting analog time-histories of torque and interpreting them according to a set of largely heuristic rules. Below we list some of the rules employed by the experts at the Draper Laboratory's Bearing Center. The rules presented here represent only the top-level rules. A purely heuristic rule-based approach to expert system design would require many more rules and sub-rules to define many of the concepts introduced in the top-level rules.

These rules were obtained by interviews with the experts. This was a tedious process which evolved over a long period of time (over six months) and required many iterations. The difficulty of obtaining such rules is well documented[26,42]. In the end, the expert system engineers themselves became experts in LSD interpretation. This was instrumental in the derivation of the system to be described.

Rule 1: A bearing is acceptable if no abnormalities (to be defined below) can be detected in the LSD torque measurement.

Rule 2: The state of assembly of the bearing must be considered in the interpretation of the LSD torque measurement.

Rule 3: The first torque measurement obtained from a new bearing determines the baseline average torque and

baseline peak-to-peak torque amplitude for that bearing.

Rule 4: The average torque and peak-to-peak torque amplitude must be less than or equal to those of the last test made on the bearing.

Rule 5: The magnitude of the average torque level must be within certain specified bounds.

Rule 6: The peak-to-peak torque amplitude must be within certain specified bounds.

Rule 7: A torque excursion is defined as a rapid variation of torque from its average value.

Rule 8: Metal damage is manifested by torque excursions of decreasing torque followed by increasing torque.

Rule 9: Particulate contamination is manifested by torque excursions of increasing torque followed by decreasing torque.

Rule 10: Misalignment of assembled bearing pairs is manifested by torque which varies sinusoidally at the rotation frequency.

This set of rules introduces concepts such as torque excursions which are very difficult for the expert to define verbally. In fact, the best description of such phenomena that the expert can give is to show examples. The engineering-based expert system approach overcomes this difficulty by applying a mixture of signal processing, spectral analysis, and pattern recognition techniques in addition to geometric and physical modeling of the torque generating mechanisms. The underlying philosophy of this approach is to unify the replication of human methods with

physical insight into the process (the mechanics of the bearings) and well established signal detection techniques. The detection of metal damage is a good example of this unification. It is known that the human expert identifies metal damage by the presence of blips of a certain shape in the torque trace, such as those shown in Figure 3-1.

Furthermore, the nature of these blips can be explained by intuitive models. An automated system capable of detecting metal damage blips must unify the visual mechanisms of the human expert and the modeled torque generating mechanism.

In addition to the interpretation rules, the expert employs some numerical criteria for acceptance of bearings. Typical acceptability criteria for an instrument bearing are listed in Table II.

3.3.2 Data Models

The signal detection and pattern recognition techniques used in the engineering-based expert system are based on data models for all of the relevant features (e.g. metal damage blips) of the torque measurement. In general, such data models may be physical (derived from principles of physics) or functional (based on observed data characteristics and statistics). In the case of the LSD procedure, intuitive physical models exist for all of the torque generating mechanisms of interest. Metal damage, particulate contamination, and poor surface quality produce geometric profile torques which have been rigorously analyzed[43]. These mechanisms are sensitive to many parameters such as the size, shape, and hardness of particles which are unknown and cannot

Table II. Typical Acceptability Criteria

CHARACTERISTIC	INDIVIDUAL BEARING SPEC.	ASSEMBLED PAIR SPEC.
AVG. TORQUE	LESS THAN 8 GM-CM	LESS THAN 16 GM-CM
PEAK TO PEAK VARIATION	LESS THAN 2 GM-CM	LESS THAN 2.8 GM-CM
PARTICULATE CONTAMINATION "BLIPS"	LESS THAN 4 PER REV. OF AMPLITUDE GREATER THAN 3 GM-CM	LESS THAN 5 PER REV. OF AMPLITUDE GREATER THAN 3 GM-CM
METAL DAMAGE "BLIPS"	NONE GREATER THAN 2 CM-GM	NONE GREATER THAN 2 GM-CM
MISALIGNMENT TORQUE AMPLITUDE	N.A.	LESS THAN 2 GM-CM

be estimated. Furthermore, the exact values of such parameters are not of interest in evaluating a bearing. Therefore, functional models are used to describe the observed LSD data. These models are discrete-time models because the automatic interpretation system will operate on digitized, sampled data.

Figure 3-2 illustrates the overall data model for the torque data produced by the LSD. The measured torque is considered the sum:

$$T_{total}(k) = T_0 + T_1(k) + T_2(k) + T_3(k) + T_4(k) \qquad (1)$$

where T_0 is the mean torque,
T_1 is the hash torque,
T_2 is the torque due to misalignment,
T_3 is the torque due to contamination,
T_4 is the torque due to metal damage, and
k is the time index

Such a model will always be possible if one component of the right-hand side of equation (1) is allowed to be an arbitrary function. In this case, the hash torque, T_1, is defined to be the component of measured torque which cannot be accounted for as mean torque, misalignment torque, particulate contamination, or metal damage. Therefore:

$$T_1(k) \equiv T_{total}(k) - T_0 - T_2(k) - T_3(k) - T_4(k) \qquad (1a)$$

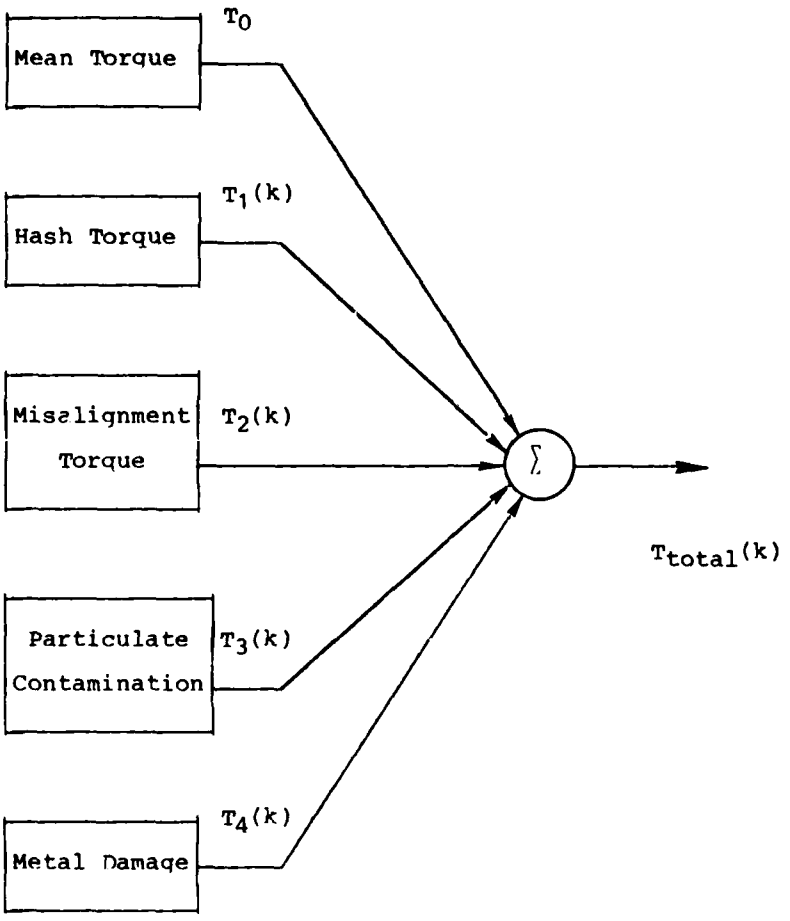

Fig. 3-2. Basic LSD Data Model

The nature of the individual torques are such that different modeling techniques are used for each. The chosen models are the basis for the detection schemes employed by the engineering-based expert system. The following models are used for these components of the torque.

Mean Torque: By definition, all other torque components are zero-mean. Therefore T_0 is the arithmetic mean of T_{total}.

Hash Torque: The hash torque is modeled as an arbitrary random noise sequence.

A convenient method to capture the statistical behavior of such a signal is the autoregressive model. The autoregressive (AR) model[44,45] is a parametric model for the behavior discrete-time signal. It is essentially a discrete linear system excited by white noise. The parameters of the system are chosen to produce desired statistics of the output. The AR model is a convenient representation for the hash torque for several reasons.

1. It is a spectral matching method. It is, in fact, an efficient method for estimating spectral densities[46].

2. Many methods exist for choosing the model parameters to optimally model a given signal.

3. The statistical behavior of a signal can be described using a finite number of model parameters, greatly reducing the data storage requirements.

4. It is a discrete linear system driven by white noise.

The AR representation for the hash torque signal $T_1(k)$ is

$$T_1(k) = -\sum_{n=1}^{p} a_n T_1(k-n) + u(k) \qquad (2)$$

where

a_n are the model parameters,
p is the model order, and
u(k) is the driving white noise.

The spectral density of an AR process given by Equation (2)

$$\Phi(w) = \frac{q}{\left| 1 + \sum_{n=1}^{p} a_n e^{-jn\omega} \right|^2} \qquad (3)$$

where q is the intensity of the input u.

The model order, p, and the model parameters, $\{a_n\}$, are chosen to match observed spectral properties of a given signal. A method for choosing the parameters is given in Appendix A. This method can be applied to LSD data which is judged to free of defects (i.e., $T_2 \equiv T_3 \equiv T_4 \equiv 0$) to estimate the parameters.

Misalignment Torque: The misalignment torque is known to be a sinusoid at the frequency of bearing rotation:

$$T_2(k) = A \cos (\Omega k \Delta t + \theta) \qquad (4)$$

where A is the misalignment amplitude and
θ is the phase of the sinusoid.
Δt is the sample interval.

Particulate Contamination and Metal Damage:

Because of their similar nature, particulate contamination and metal damage can be modeled similarly. They will be modeled as a low-density shot noise process[47,48]. The general shot noise process is

$$s(t) = \sum_i b_i \, h(t-t_i) \qquad (5)$$

where $h(\cdot)$ is a given function,

$\{t_i\}$ is a set of Poisson points, and

$\{b_i\}$ is a set of purely random variables independent of $\{t_i\}$.

An interpretation of the shot noise process is a series of time functions, h(t), occurring at random times. For the purpose of modeling metal damage and particulate contamination "blips," the function h(t) can represent the shape of such a blip, t_i will represent the unknown times of occurence of the blips, and b_i will represent blip intensities. To formulate a discrete-time shot noise process, we require that the sampling interval, Δt, is small enough so that

$$\lambda \Delta t \ll 1 \qquad (6)$$

where λ is the Poisson parameter (average density of events) a series approximation of the Poisson probability function given by (47)

$$P_n(t) = \Pr\{n \text{ events in time period } t\} = \frac{(\lambda t)^n}{n!} e^{-\lambda t} \tag{7}$$

can be stated as

$$P_0(\Delta t) \simeq 1 - \Delta t \tag{8}$$

$$P_1(\Delta t) \simeq \lambda \Delta t$$

$$P_n(\Delta t) \simeq 0 \quad n>1$$

The physical interpretation of this condition is that no more than one event (blip) may occur during one sample interval, Δt. Furthermore, the probability that an event will occur during any sample interval is $\lambda \Delta t$.

3.3.3 Detection Algorithms

Given the LSD data models described in the previous section and illustrated in Figure 3-2, the first function of the engineering-based expert system is to decompose the torque measurement, T_{total}, into its relevant components. The algorithms to perform this decomposition are signal processing algorithms based on the models for individual torque components. The requirements of these algorithms are stated below.

1. The system will operate on digitized data sampled with uniform sampling period Δt.

2. The computations do not need to be performed in real-time, therefore we are not restricted to real-time, casual systems.

3. The results of the processing algorithms must be: the value of the mean torque, the number and magnitudes of particulate contamination and metal damage blips, the magnitude of misalignment torque, and the amplitude and spectral properties of the hash torque.

The architecture of the system is illustrated in Figure 3-3. The overall approach is subtractive - individual torque components are estimated and removed from the data in succession.

The data is assumed to consist of finite records of N samples of torque sampled with period Δt. The individual signal processing techniques are described below.

Mean torque: The estimated mean torque, $\hat{T}_o$ is the sample mean of T_{total}.

$$\hat{T}_o = \frac{1}{N} \sum_{i=0}^{N-1} T_{total}(k)$$

Misalignment Torque: The misalignment torque is a sinusoidal torque of a known frequency. Therefore, its amplitude and phase may be estimated by a Fourier decomposition of T_{total}.

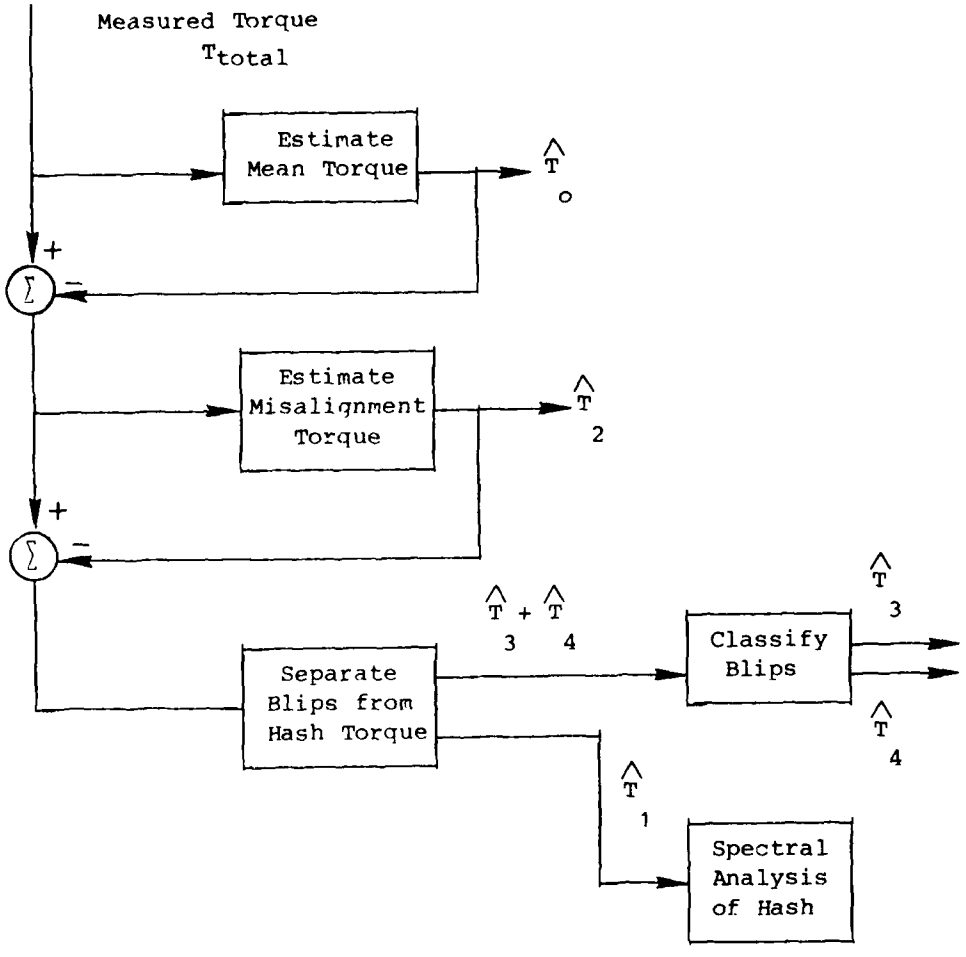

Fig. 3-3. Architecture of System

$$\hat{T}_2(k) = A \cos(\Omega\Delta t + \theta) \qquad (10)$$

$$= B \cos \Omega\Delta t + C \sin \Omega\Delta t$$

where

$$A = \sqrt{B^2 + C^2}$$

$$\theta = \tan^{-1}(C/B)$$

$$B = \frac{2}{N} \sum_{i=0}^{N-1} \cos(\Omega_r i \Delta t) \left[T_{total}(i) - \hat{T}_o \right] \qquad (11)$$

$$C = \frac{2}{N} \sum_{i=0}^{N-1} \sin(\Omega_r i \Delta t) \left[T_{total}(i) - \hat{T}_o \right] \qquad (12)$$

Separation of Hash Torque from Metal Damage and Particulate Contamination

Having detached the mean torque and misalignment torque, the remaining task is to separate the blips from the hash torque. Based on the expert's definition of torque excursion as a rapid torque variation, a threshold detection algorithm can be used to distinguish blips from hash torque. Using the symbol Z(k) to denote the torque measurement without mean or misalignment;

$$Z(k) = T_1(k) + T_3(K) + T_4(k) \tag{13}$$

and the symbol V(k) to denote blips of both types:

$$V(k) = T_3(k) + T_4(k) \tag{14}$$

we may write

$$Z(k) = T_1(k) + V(k) \tag{15}$$

The AR model, equation (2), may be used as a predictor for the hash torque:

$$\hat{T}_1(k) = -\sum_{n=1}^{p} a_n T_1(k-n) \tag{16}$$

and a pseudo-measurement, $Z^1(k)$, can be created,

$$\begin{aligned} Z^1(k) &= Z(k) - \hat{T}_1(k) \\ &= V(k) + U(k) \end{aligned} \tag{17}$$

which consists only of blips and white noise. We may then apply a threshold to the pseudo-measurement to detect blips on the basis of their magnitude:

$$\hat{V}(k) = \begin{cases} Z^1(k) - \gamma \text{ if } Z^1(k) > \gamma \\ 0 \quad \text{if} \quad |Z^1(k)| \leq \gamma \\ Z^1(k) + \gamma \text{ if } Z^1(k) < -\gamma \end{cases} \tag{18}$$

where γ is a predetermined threshold. The threshold value must be selected according to the magnitude of the blips which must be detected and the known statistics of the white noise, U(k). Because only estimates of the hash torque are available, we must create an updated estimate,

$$\bar{T}_1(k) = Z(k) - \hat{v(k)} \tag{19}$$

to drive the predictor:

$$\hat{T}_1(k) = -\sum_{n=1}^{p} a_n \bar{T}(k-n) \tag{20}$$

$\hat{T}_1(k)$ is an a priori estimate of the hash torque because it is made without knowledge of any measurement. $\bar{T}_1(k)$ is an a posteriori estimate of the hash torque because it is made after the measurement is available. This nonlinear filtering scheme is illustrated in Figure 3-4. A more detailed derivation

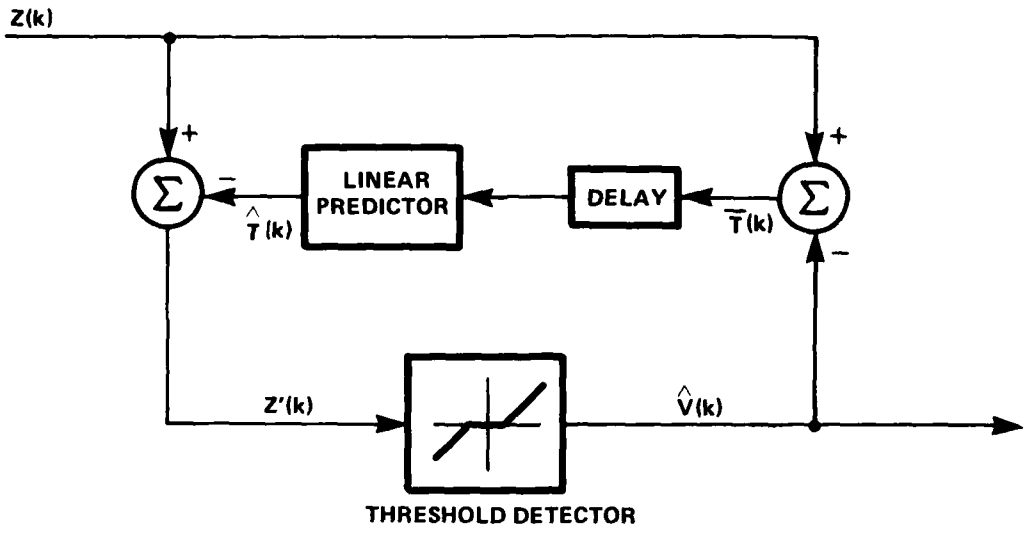

Fig. 3-4. Nonlinear Filter for Detecting Metal Damage and Particulate Contamination Artifacts

is given in Appendix B. Typical output is illustrated in the lower plot of Figure 3-5.

The principle of operation for the filter is that the AR predictor, equation (20), is used as a whitening filter to reduce the amplitude of the hash torque before applying the threshold.

The detection algorithms are summarized in Table III.

Work is ongoing to apply statistical pattern recognition techniques to the problem of detecting metal damage and particulate contamination. A master of science thesis is in progress which will apply the Karhunen-Loéve method of feature extraction[49]. This method will permit the detection of arbitrary signals based on a learning set provided by the experts. In this way, the process of describing such signals heuristically can be circumvented. This thesis will be completed by August 1985.

3.4 Performance of the LSD Analysis System

The detection algorithms described in the previous section are combined in a software architecture illustrated in Figure 3-6. The analysis software was written in the C programming language and currently runs on an IBM XT personal computer. C is an efficient, modular and structured general purpose programming language. Its flexibility allows it to be useful for low-level data input as well as high-level graphics routines.

The torque data from the dynamometer is sampled and digitized at 50 Hz. The dynamometer has a bandwidth of about 18 Hz (see Appendix C). The first operation of the system is to calculate the sample mean and variance of the torque measurement. A bearing can be rejected if the mean torque or torque variance is too large. The mean and variance are not, however, sufficient to identify the nature of the failure. The second element of the

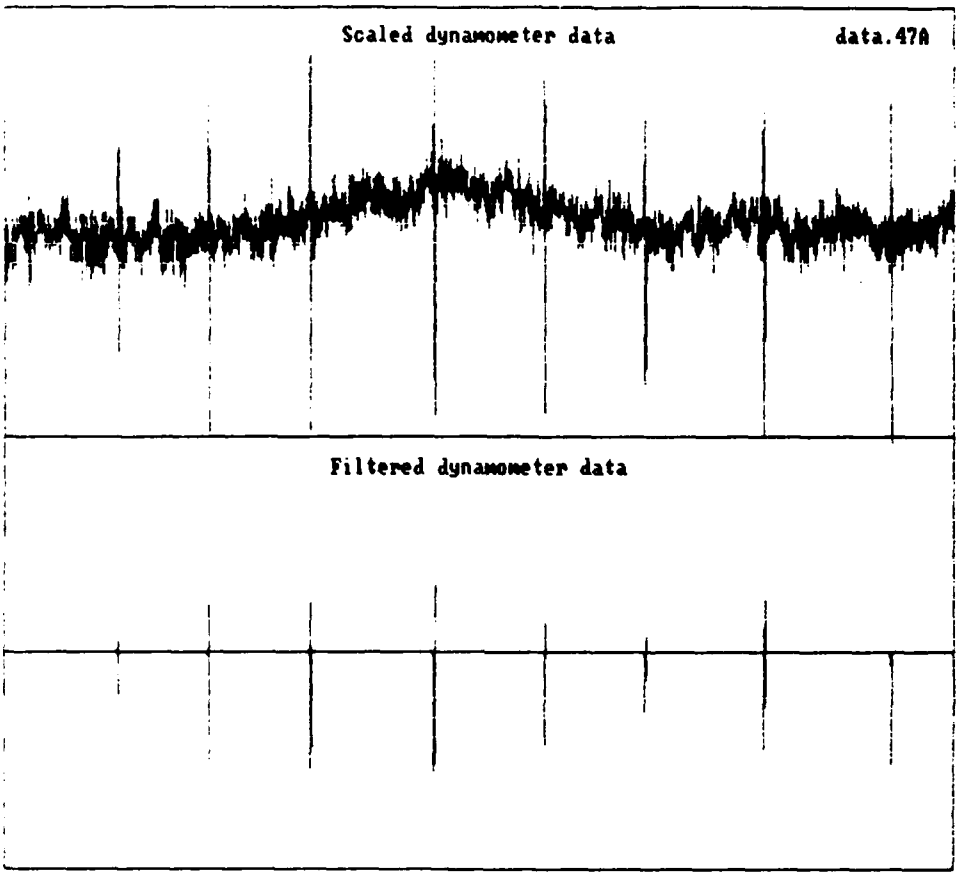

Fig. 3-5. Typical LSD Data: Raw and Filtered

Table III. Detection Algorithms

CONDITION	SYMPTOMS	EQUATION	FAILURE RULE
Excessive torque or improper preload	Mean torque out of range	$\bar{\tau} = \frac{1}{N} \sum_{n=1}^{N} \tau_n$	$\bar{\tau} < \tau_{min}$ $\bar{\tau} > \tau_{max}$
Lubricant degradation or poor surface finish	Torque variance too large	$\sigma^2 = \frac{1}{N} \sum_{n=1}^{N} (\tau_n - \bar{\tau})^2$	$\sigma^2 > \sigma^2_{max}$
Particulate contamination or metal damage	Blips	$z_n = F\left\{\tau_n + \sum_{j=1}^{p} c_j z_{n-j}\right\}$ $F\{\cdot\}$ = threshold function c_j = autoregressive parameters	$z_n \neq 0$
Misalignment	Sinusoidal torque variation	$A = \left\lvert \frac{2}{N} \sum_{n=1}^{N} \tau_n e^{-j\Omega nT} \right\rvert$ Ω = rotation frequency	$A \geq A_{max}$

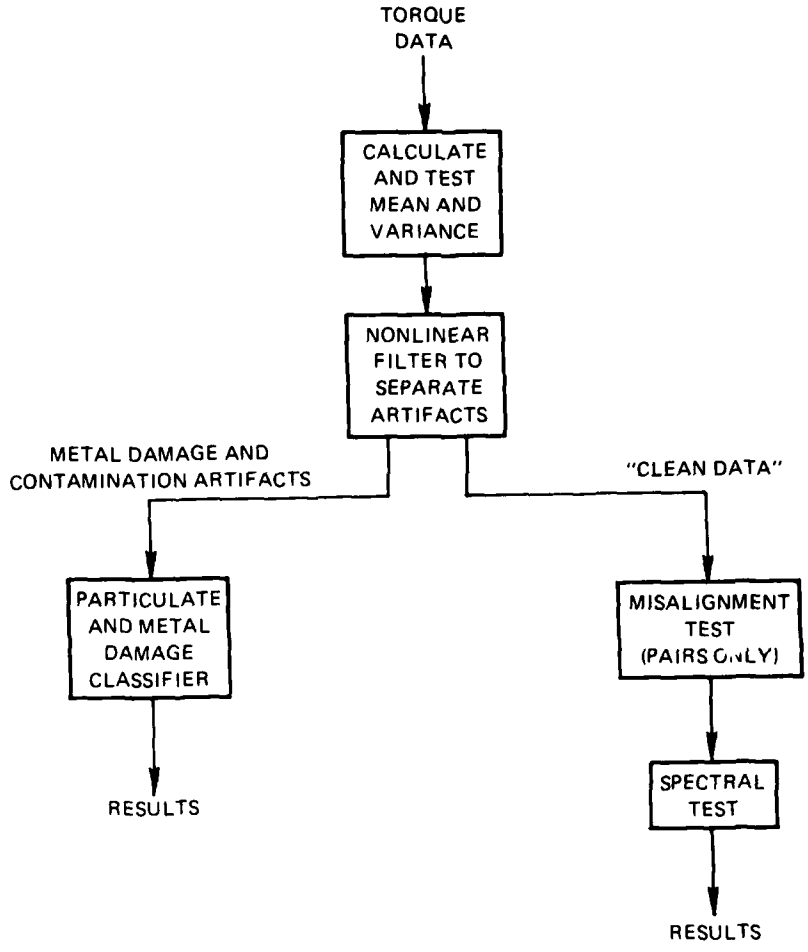

Fig. 3-6. Software System Architecture

system is the nonlinear filter to detect and remove artifacts due to metal damage and particulate contamination. Running totals of the number of such artifacts are maintained. The remaining torque data (after removal of the metal damage and contamination blips) are tested for misalignment (if appropriate) and then tested for excessive amplitude in two frequency bands - above and below 1 Hz. The signal below 1 Hz contains the effects of race out-of-roundness and misalignment. Misalignment is detected as described in the previous section. The signal above 1 Hz contains the effects of lubricant degradation and poor surface finish - the causes of "hash." The bearing will be rejected if the average amplitude in either of these frequency bands exceeds preset values.

The analysis system has been throroughly tested on over 50 digitized LSD torque traces from routine tests of G-Star Momentum Wheel ball bearings at various stages of their assembly. The automatic analyses have been consistent with the judgement of the experts. Appendix D contains a summary of the automatic analyses. The analysis system has exhibited a more sensitive threshold of detection. This, as a consequence, has heightened sensitivity to the issue of how the LSD test results relate to bearing life. Previously, the criteria of acceptability were based solely on the sensitivity limit of the expert. The expert rejected a bearing if he could detect any artifacts of failure modes. As greater sensitivity can be achieved, however, the criteria of acceptability must be adjusted to reflect the actual operational requirements of the bearing rather than the limits of artifact detectability.

Sample output from one LSD analysis is shown in Figures 3-5 and 3-7. The upper trace of Figure 3-5 shows the raw dynamometer data from one test on a bearing. The torque signal contains both low and high frequency components as well as blips. These blips are indicitive of either metal damage of particulate contamination. The lower trace is the torque data after the nonlinear filter and threshold detection have been applied. Here, only the spikes remain; the low and high frequency components are subtracted from the upper trace. This portion of the signal is

```
        LOW SPEED DYNAMOMETER
      BEARING ANALYSIS PROGRAM
            Version 2.0

Friday December 20, 1985                File: data.47A

TEST INFORMATION

   Configuration: DUMMY WHEEL      Bearing ID(s): 124 B   130 B
   Direction: CCW                  Load:    9.000
   Preamp atten: x4                Transducer sens:    4.000
   Operator: SB                    Moment arm: 1

MEAN TORQUE TEST

   measurement:  mean torque value
   value:        9.377427
   decision:     mean value within bounds

TORQUE VARIANCE TEST

   measurement:  variance of torque
   value:        1.121466
   decision:     variance out of bounds

BLIP DETECTION & CLASSIFICATION

   8 violations:   7 Metal damage
                   0 Particulate contamination
                   1 Undetermined blips

   METAL DAMAGE
   point 726       max:   0.39 min:  -1.78
   point 1296      max:   1.87 min:  -4.55
   point 1938      max:   1.98 min:  -4.78
   point 2722      max:   2.64 min:  -4.89
   point 3419      max:   1.13 min:  -3.78
   point 4054      max:   0.57 min:  -2.43
   point 4804      max:   2.04 min:  -3.97

   UNDETERMINED BLIPS
   point 5606      max:   0.00 min:  -4.55

POWER SPECTRUM ANALYSIS

   measurement:  amplitude < 1 Hz
   value:        0.990287
   decision:     excessive amplitude

   measurement:  amplitude > 1 Hz
   value:        1.372677
   decision:     excessive amplitude

MISALIGNMENT TEST

   measurement:  sinusoidal amp 1/60 Hz
   value:        0.124058
   decision:     misalignment not detected
```

Fig. 3-7. Summary Results for a Typical LSD Analysis

analyzed by the blip detection algorithm. The clean data (raw torque data minus the blips) is analyzed for misalignment (on bearing pairs) and is spectrally analyzed in a low and high frequency band.

Figure 3-7 is a summary of the test results. The top of the summary contains information which uniquely identifies the bearing and the LSD test parameters. The result of the mean torque test is shown next. In this case the mean torque is within acceptable limits. The torque variance, however, is too high. This fact would have been visually recognized by the experts and the bearing would have been rejected. The results of the blip detection and classification algorithm indicate that the seven of the eight blips shown in Figure 3-5 are a result of metal damage and one blip cannot be positively identified as either metal damage or particulate contamination. The misalignment test is not performed since only a single bearing is tested (i.e., not a bearing pair). The power spectral analysis indicates excessive amplitude in both low and high frequency bands. The analysis of the LSD test indicates the bearing is damaged. The torque variance, metal damage blips and excessive amplitude render this bearing unacceptable. The bearing must be dismantled, cleaned and the source of metal damage identified.

The analysis results of an acceptable bearing are shown in Figures 3-8 and 3-9. The torque traces (Figure 3-8) show and the summary information (Figure 3-9) confirm that this bearing contains no metal damage or particulate contamination. The bearing is within acceptable limits in the other tests: mean torque, torque variance and power spectral analysis. This bearing is acceptable and would have continued in its integration into a component.

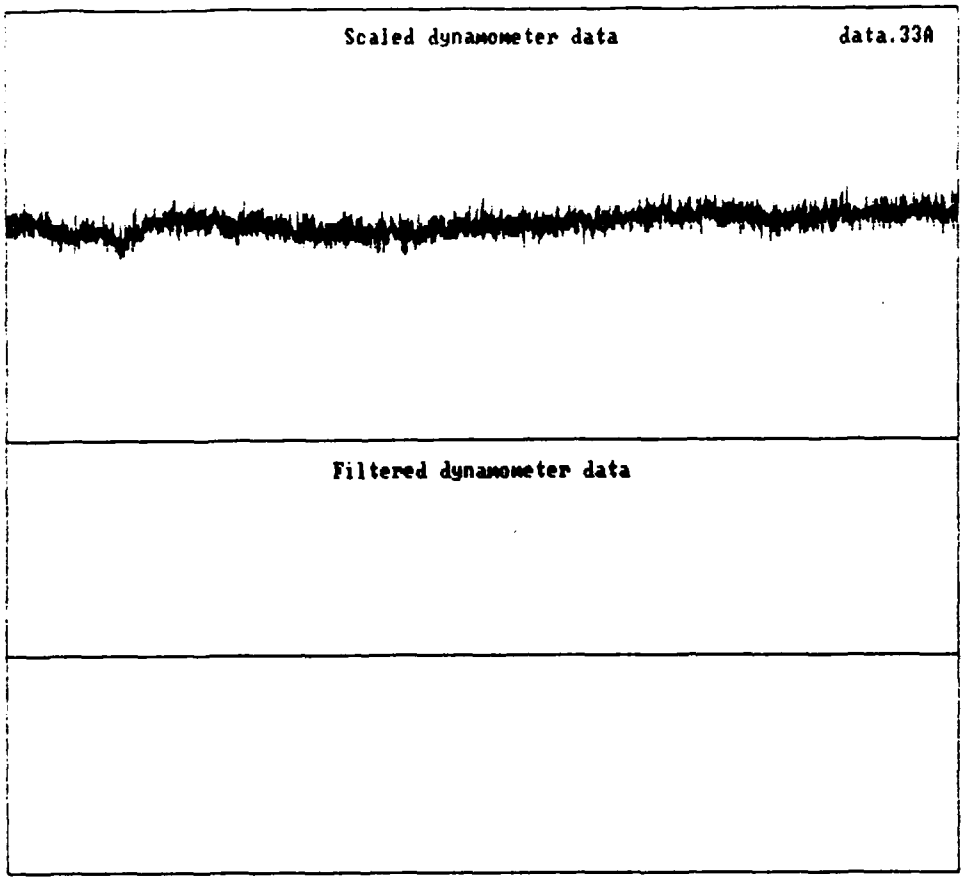

Fig. 3-8. Acceptable LSD Data: Raw and Filtered

LOW SPEED DYNAMOMETER
BEARING ANALYSIS PROGRAM
Version 2.0

Friday December 20, 1985 File: data.33A

TEST INFORMATION

Configuration: SINGLE	Bearing ID(s): 131 B
Direction: CCW	Load: 9.000
Preamp atten: X5	Transducer sens: 4.000
Operator: JL	Moment arm: 1

MEAN TORQUE TEST

measurement:	mean torque value
value:	6.537896
decision:	mean value within bounds

TORQUE VARIANCE TEST

measurement:	variance of torque
value:	0.160510
decision:	variance within bounds

BLIP DETECTION & CLASSIFICATION

0 violations:	0 Metal damage
	0 Particulate contamination
	0 Undetermined blips

POWER SPECTRUM ANALYSIS

measurement:	amplitude < 1 Hz
value:	0.767208
decision:	acceptable excessive
measurement:	amplitude > 1 Hz
value:	1.083914
decision:	acceptable amplitude

Fig. 3-9. Summary Results of an Acceptable LSD Analysis

4.0 CONCLUSIONS AND RECOMMENDATIONS

4.1 Conclusions of Present Research

The original hypothesis of constructing intelligent modules for non-deterministic tasks with control system engineering and artificial intelligence techniques has been explored. Results from this exploration have been twofold: the development of the engineering-based expert system method of analysis and the demonstration of this method in automating a complex task typically performed by a human expert.

The engineering based expert system has been shown to be effective in solving a certain class of problems. Problems characterized as falling in between those for which mathematical process models exist and those described completely by human expertise are amenable to this approach. There are a great many of these "partially analyzable" problems that exist where this approach should prove interesting.

One such task, that of inspection of precision ball bearings, has been automated using the principles of the engineering-based expert system. The automated system has been demonstrated to be as sensitive to bearing defect artifacts as the expert is. The system will be undergoing extensive development and improvement over the next year because funding has been received to install the ball bearing inspection system on the factory floor of one of the Navy's suppliers of precision mechanisms.

4.2 Recommendations for Further Research

The promising nature of the engineering-based expert system methodology and its successful application to a complicated inspection task leads us to consider extending our work into two different directions: horizontally, across tasks different than inspection of precision ball bearings; and vertically, deeper into ball bearing manufacture. In other words, use the automatic data interpretation work as an entry to explore the research issues for an intelligent manufacturing system for bearings.

The engineering-based expert system method is generic in the sense that is can be applied to a range of problems. We have chosen one particular task to test the method. The LSD interpretation fits into a category of problems which are analyzed by a combination of mathematical and intuitive models and human heuristics. We feel that there are many problems similar to the ball bearing inspection problem which can be automated using the developed methods.

Analysis of low-speed dynamometer tests give detailed information concerning the specific condition of the bearing. The bearing, at the time it is tested by the LSD, has undergone many manufacturing processes. All of these processes contribute to the final condition of the bearing at the time it is tested. The stages of manufacturing of a bearing and the attributes associated with them are illustrated in Figure 4-1. Bearing attributes can be categorized into types, principal and physical. Principal attributes are characterized by component mechanics, surface chemistry, materials and metrology. Physical attributes are specifically related to the manufacture of the balls and races. Attributes which fall into this category are clamping methods, types of tools and materials and processing data like treatments. While the LSD has been designed to test the bearing after all the manufacturing processes have been completed, it is thought that it also contains information that can be related to the physical attributes of bearing manufacture. Specific research issues include whether the analysis of LSD data provides information concerning the manufacturing of the bearing in addition to information regarding the specific condition of the bearing. If so, the LSD may be used as a feedback mechanism in the entire bearing manufacturing process. The use of the LSD in this manner is an interesting area for future research.

The research hypothesis is that the low-speed dynamometer test data contains significant information that can be related directly to attributes of bearing manufacture. Whether there is enough information to successfully control the manufacturing

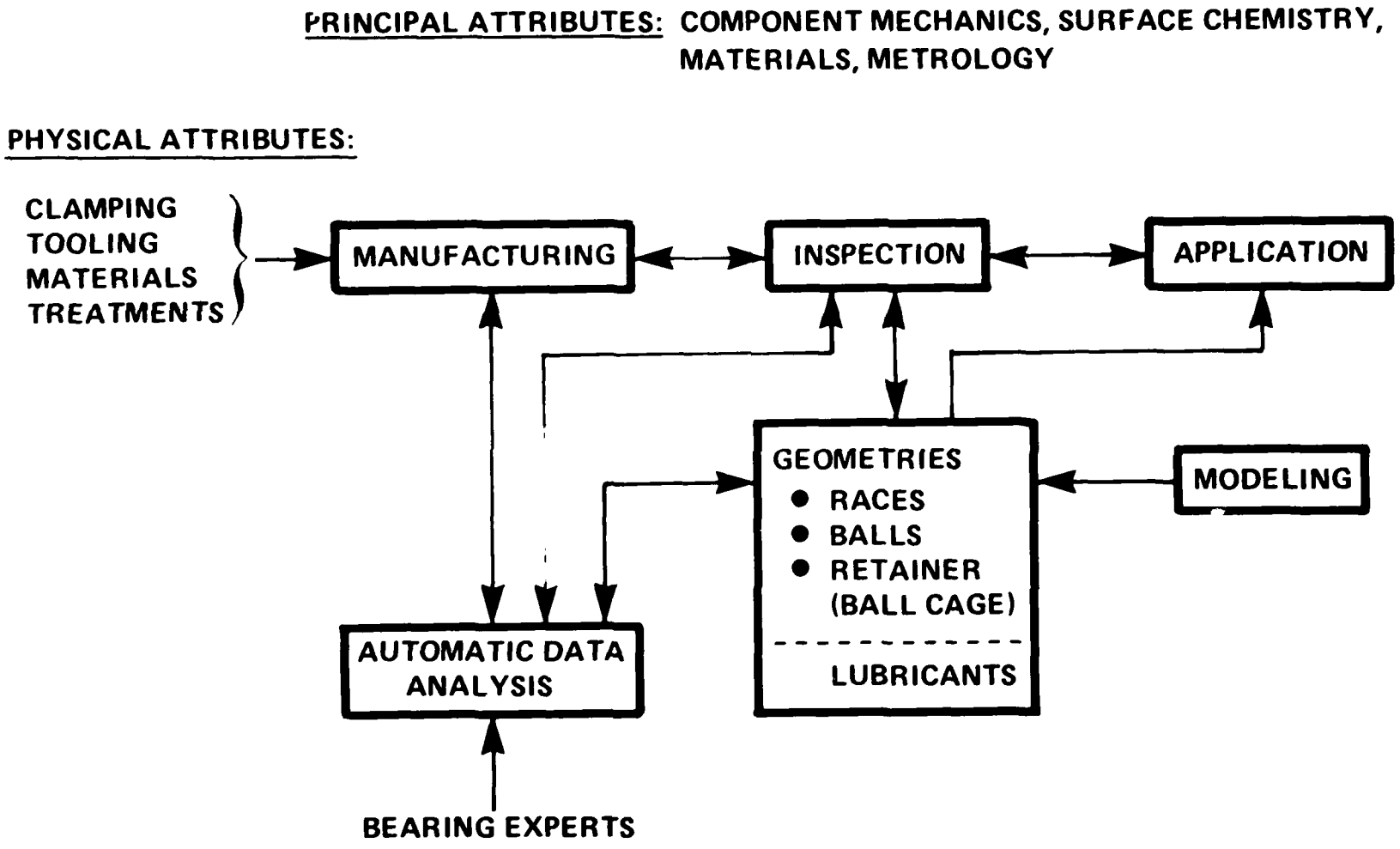

Fig. 4-1. Relationship of Principal and Physical Attributes in Bearing Manufacture

processes is one of the key research questions. Also types and needs of additional information sources would also be a key ingredient of a research program to explore these issues.

REFERENCES

1. "Exploratory Research in Industrial Modular Assembly," by J.L. Nevins, et al.; a series of reports published by CSDL from 1972-1979. Report No.'s are R-800, R-837, R-850, R-921, R-996, R-1111, R-1218, R-1276, R-1284.

2. Adams, M.B., O.L. Duetsch, J.L. Harrison, "A Hierarchical Planner for Intelligent Systems," a paper presented at the SPIE Conference on Applications of A.I., Crystal City, VA, April 11-12, 1985. Also published as CSDL Report P-2014, March 1985.

3. Deutsch, O.L., J.L. Harrison, M.B. Adams, "Heuristically-Guided Planning for Mission Control/Decision Support," CSDL Report P-2052, June 1985.

4. Naito, K., "Control of Automatic Assembly Line for Wrist Watches, 'System A'", Precision Instruments, Vol. 38, No. 1, pp. 114-119, January 1972.

5. Dunne, M.J., "An Assembly Experiment Using Programmable Robot Arms," Proceedings 7th International Symposium on Industrial Robots, Tokyo, Japan, pp. 387-397, 1977.

6. Akiyama, J., "Flexible Assembly Center System - FX-1," a presentation made at the 2nd Annual Seminar on Advanced Assembly Research, "The Charles Stark Draper Laboratory, Inc., November 1981.

7. Nevins, J.L., T.B. Sheridan, D.E. Whitney, "Flexible Automation, A First Concept," MIT CSDL Report E-2707, August 1972, presented at the IEEE NEREM meeting on November 2, 1972.

8. Nevins, J.L., D.E. Whitney, "The Force Vector Assembler Concept," MIT CSDL Report E-2754, April 1973, presented at the first CIS-IFTOMM Symposium on Theory and Practice of Robots and Manipulators, Udine, Italy, September 5-8, 1972.

9. Whitney, D.E., J.L. Nevins, "Servo Controlled Mobility Device," U.S. Patent No. 4,156,835, issued 29 May 1976 - filed 29 May 1974.

10. Whitney, D.E., J.L. Nevins, "Servo Controlled Mobility Device," U.S. Patent No. 4,243,923, issued January 6, 1981, filed January 22, 1979.

11. Watson, P.C., "A Multidimensional System Analysis of the Assembly Process as Performed by a Manipulator," presented at the First North American Robot Conference, Chicago, 1976.

12. Watson, P.C., "Remote Center Compliance," U.S. Patent No. 4,098,001, issued July 4, 1978 - filed October 13, 1976.

13. Goto, T., T. Inoyama, K. Takeysau, "Precise Insert Opposition by Tactile Controlled Robot Hi-T-Hand 'Expert 2'", Proceedings 4th International Symposium on Industrial Robots, pp. 209-218, 1974.

14. Gustavson, R.E., "A Theory for the Three Dimensional Mating of Chamfered Cylindrical Parts," ASME Paper 84-DET-115.

15. Gustavson, R.E., "Operator Member Erection System and Method," U.S. Patent No. 4,324,032, issued April 13, 1982 - filed May 5, 1980.

16. Seltzer, D.S., Tactile Sensory Feedback for Difficult Robot Tasks," presented at the Robots VI Conference, March 2-4, 1982, and published as SME Paper MS-82-220.

17. Watson, P.C., "Instrumented Remote Center Compliance," U.S. Patent No. 4,316,329, issued February 23, 1982 - filed September 19, 1979.

18. Watson, P.C., S.H. Drake, "Pedestal and Wrist Force Sensors for Automatic Assembly," presented at the 5th ISIR, ITT, Chicago, IL., September 22-24, 1975, also published as CSDL Report P-176, June 1975.

19. Watson, P.C., "Method and Apparatus for Six Degree of Freedom Force Sensing," U.S. Patent No. 4,094, 192, issued June 13, 1978 - filed September 20, 1976.

20. Nevins, J.L., et al., "Adaptive Control, Learning and Cost Effective Sensor Systems for Robotics or Advanced Automation Systems,", 1st Annual Progress Report covering the period August 1, 1983 - July 31, 1984, CSDL Report R-1756.

21. Nevins, J.L., A.C. Edsall, M.E. Kaliski, T.M. Stepien, "Automatic Interpretation of Low-Speed Dynamometer (Torque) Traces of Precision Ball bearings by an Engineering-Based Expert System," CSDL Report P-2042, May 1985.

22. Nevins, J.L. et. al., First Annual Progress Report, "Adaptive Control, Learning and Cost-Effective Sensor Systems for Robotic or Advanced Automation Systems," First annual Report, covering period March 31, 1983 to March 31, 1984, CSDL Report R-1757.

23. Laming, T.W., "A Perturbation Approach to Surface Estimation," S.M. Thesis, Department of Aeronautics and Astronautics, Massachusetts Institute of Technology, August 1984.

24. Singer, H.B., "Innovative Features of Long Life Momentum and Reaction Wheel Assemblies," presented at IFAC 8th Triennial World Congress, August 24-28, 1981, Kyoto, Japan. Also published as CSDL Report P-1304, May 1981.

25. Mylopoulos, J., "An Overview of Knowledge Representation," Proceedings Workshop on Data Abstraction, Databases, and Conceptual Modeling, Association for Computing Machinery, June 23-26, 1980.

26. Hayes-Roth, F., D.A. Waterman, D.B. Lenat (eds.), Building Expert Systems, London, Addison-Wesley, 1983.

27. Davis, R., B. Buchanan, E. Shortliffe, "Production Rules as a Representation for a Knowledge-Based Consultation Program, Artificial Intelligence, Vol. 8, No. 1, 1977.

28. Feigenbaum, E.A., "The Art of Artificial Intelligence: Themes and Case Studies of Knowledge Engineering," Proceedings 1977 IJCAI, pp. 1014-1029.

29. Young, T.Y., T.W. Calvert, Classification, Estimation, and Pattern Recognition, New York, American Elsevier Publishing Co., Inc., 1974.

30. Bonisone, P.P., H.E. Johnson, Jr., "Expert System for Diesel Electric Locomotive Repair," Proceedings 1983 IJCAI.

31. Dixon, J.R., M.K. Simmons, "Expert Systems for Engineering Design: Standard V-Belt Drive Design as an Example of the Design-Evalute-Redesign Architecture," Proceedings 1984 ASME Computers in Engineering Conference.

32. Shen-Orr, C.D., "Automatic Design of Complex Gear Trains," Sc.D. Thesis, Massachusetts Institute of Techology, June 1976, also CSDL Report T-627.

33. Rychener, M.D., "Expert Systems for Engineering Design: Experiments with Basic Techniques," Proceedings 1983 IEEE Design Automation Conference, pp. 21-27.

34. Kunz, J.C., "Use of Artificial Intelligence and Simple Mathematics to Analyze a Physiological Model," Ph.D. Dissertation, Stanford University, Department of Computer Science, June 1984.

35. Kaemmerer, W.F., P.D. Christopherson, "Using Process Models with Expert Systems to Aid Prcess Control Operators," Proceedings 1985 American Control Conference, pp. 892-897.

36. Bernard, J.A., A. Ray, K.S. Kwok, D.D. Lanning, "Design and Experimental Evaluation of a 'Fuzzy' System for Control of Reactor Power," Proceedings 1985 American Control Conference, pp. 1466-1474.

37. Yager, R., "Towards a General Theory of Reasoning with Uncertainty," IEEE Workshop on Intelligent Control, Rensselaer Polytechnic Institute, August 26-27, 1985.

38. Oppenheim, A.V. (ed.), Applications of Digital Signal Processing, Englewood Cliffs, Prentice-Hall, Inc., 1978.

39. Therrien, C.W., "A Sequential Approach to Target Discrimination," IEEE Transactions on Aerospace and Electronic Systems, Vol. AES-14, No. 3, May 1978.

40. Halliday, J.S., "The Characterization of Vectorcardiograms for Pattern Recognition," S.M. Thesis, Massachusetts Institute of Technology, Department of Electrical Engineering, May 1973, also CSDL Report T-583.

41. "A Guide for Selection and Application of Precision Instrument Ball Bearings," CSDL Report R-1010, October, 1976.

42. Gaglio, S., R. Minciardi, and P.P. Puliofito, "Multiperson Decision Aspects in the Construction of Expert Systems," IEEE Trans. Systems, Man, and Cybernetics, Vol. SMC-15, No. 4, July/August 1985.

43. Francis, H., "BEARDYN - A Computer Model for Geometrically Imperfect Ball Bearings," CSDL Report R-1713, November 1984.

44. Box, G.E.P., and G.M. Jenkins, Time Series Analysis, San Francisco, Holden-Day, 1974.

45. Makhoul, J. "Linear Prediction: A Tutorial Review," Proceedings IEEE, Vol. 63, No. 4, April 1975.

46. Papoulis, A., "Maximum Entropy and Spectral Estimation: A Review," IEEE Transactions on Acoustics, Speech, and Signal Processing, Vol. ASSP-29, No. 6, December 1981.

47. Papoulis, A., Probability, Random Variables, and Stochastic Processes, New York, McGraw-Hill, 1984.

48. Laning, J.H. and R.H. Battin, Random Processes in Automatic Control, New York, McGraw-Hill, 1956.

49. Young, T.Y., and T.W. Calvert, Classification, Estimation, and Pattern Recognition, New York, Elsevier Publishing Co., 1974.

APPENDIX A

AUTOREGRESSIVE PROCESSES

The AR process is a convenient parametric model for the behavior of a signal. It belongs to a more general class of discrete processes known as linear predictors(45,46). The linear prediction model approximates a signal s(n) as the output of a linear filter driven by white noise.

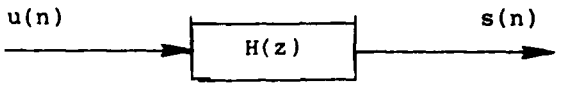

The filter transfer function is assumed to be of the rational form

$$H(z) = \frac{\sum_{l=0}^{q} b_l z^{-l}}{1 + \sum_{k=1}^{p} a_k z^{-k}} \qquad \text{(A-1)}$$

The corresponding difference equation is

$$s(n) = -\sum_{k=1}^{p} a_k s(n-k) + \sum_{l=0}^{q} b_l u(n-l) \qquad \text{(A-2)}$$

which shows that s(n) is a linear combination of past outputs and past and present inputs. If q=0, then Equation (A-1) is an all-pole or infinite impulse response filter and s(n) is an AR process.

$$s(n) = \sum_{k=1}^{p} a_k s(n-k) + b_o u(n) \qquad \text{(A-3)}$$

Finally, note that because u(n) is assumed to be zero mean white noise, the optimal estimate of s(n) from past values is

$$\hat{s}(n) = -\sum_{k=1}^{p} a_k s(n-k) \tag{A-4}$$

Equation A-4 illustrates the use of the AR model as a linear predictor. The prediction error or residual is

$$e(n) = s(n) - \hat{s}(n) = b_o u(n) \tag{A-5}$$

Parameter Estimation

Given a signal s(n) to be modeled as an AR process, the parameters a_k are chosen to minimize the mean square prediction error

$$E\left[e^2(n)\right] = E\left[\left(s(n) + \sum_{k=1}^{p} a_k s(n-k)\right)^2\right] \tag{A-6}$$

$$E\left[e^2(n)\right] = E\left[s^2(n)\right] + 2\sum_{k=1}^{p} a_k E\left[s(n)s(n-k)\right] + \sum_{k=1}^{p} a_k \sum_{l=1}^{p} a_l E\left[s(n-k)s(n-l)\right] \tag{A-7}$$

Necessary conditions for minimization are

$$\frac{\partial}{\partial a_k} E\left[e^2(n)\right] = 0 \qquad k = 1 \ldots p \tag{A-8}$$

from which we obtain

$$2E\left[s(n)s(n-k)\right] + 2\sum_{l=1}^{p} a_l E\left[s(n-l)s(n-k)k\right] = 0 \tag{A-9}$$

If s(n) is a stationary signal, its autocorrelation function is

$$R_s(m) = E\left[s(n)s(n-m)\right] \tag{A-10}$$

so that Equation (A-9) reduces to

$$\sum_{l=1}^{p} a_l R_s(l-k) = -R_s(k) \tag{A-11}$$

to be solved for k=1, 2 ..., p. These are the normal equations(45).

Parameter Estimation from Noisy Measurements

The AR coefficients may be computed from the normal equations (A-11) given an estimate of the first p terms of the autocorrelation function. In a more general problem, it is desired to fit an AR model to a signal s(n) given a measurement

$$z(n) = hs(n) + v(n) \tag{A-12}$$

where h is a known parameter and v(n) is white noise.

The measurement noise has the property that

$$E\left[v(n)v(k)\right] = r\delta_{nk} \tag{A-13}$$

$$E\left[v(n)s(k)\right] = 0 \tag{A-14}$$

The autocorrelation function for the measurement is

$$\begin{aligned} R_z(m) &= E\left[(hs(n) + v(n))\,(hs(n-m) + v(n-m))\right] \\ &= h^2 E\left[s(n)v(n)\right] + E\left[v(n)v(n-m)\right] \\ &\quad + hE\left[s(n-m)v(n)\right] + E\left[v(n)v(n-m)\right] \\ &= h^2 R_x(m) + r\delta_{om} \end{aligned} \tag{A-15}$$

The normal equations may be rewritten in terms of the experimentally obtainable measurement autocorrelation R_z as

$$\sum_{l=1}^{p} a_l \left[R_z(l-k) - r\delta_{lk} \right] = -R_z(k), \quad k=1, \ldots, p \qquad \text{(A-16)}$$

APPENDIX B

THRESHOLD DETECTION OF METAL DAMAGE AND PARTICULATE CONTAMINATION

This appendix describes a method of identifying suspected particulate contamination and metal damage artifacts in low-speed dynamometer (LSD) torque measurements. The method is based on threshold detection with particular attention to the selection of the threshold value and to the reliabiity of the test. An extension is made to take advantage of correlation in the measurements. It is proposed that this algorithm can be used to locate suspicious features in the torque measurement as a "front-end" for a more powerful pattern classifier.

Figures B-1 and B-2 show an acceptable LSD torque measurement and one exhibiting metal damage artifacts. The metal damage is characterized by almost periodic "spikes" in the torque as the damaged metal area is contacted by a mating ball or race. Particulate contamination produces a spike that is similar but of opposite magnitude. Figures B-3 and B-4 show metal damage and particulate contamination artifacts, respectively, on an expanded time scale. The method described here is developed under the assumption that the detection of these artifacts can be approximated by or reduced to (by deconvolution, for example) the problem of detecting impulses in random noise.

Stochastic Modelling of LSD Torque Measurements

The torque measurement, $z(t)$, will be modelled as the sum of a continuous random variable, $w(t)$, and a series of random impulses, $v(t)$;

$$z(t) = w(t) + v(t) \tag{B-1}$$

where $w(t)$ has a known probability density function (PDF), $p_w(x)$, and $v(t)$ is the "shot effect"[46,47] defined by

$$v(t) = \sum_j a_j \delta(t-t_j) \tag{B-2}$$

where a_j are random intensities and
t_j are Poisson distributed event times.

The intensities, a_j, have a known PDF, $p_a(x)$.

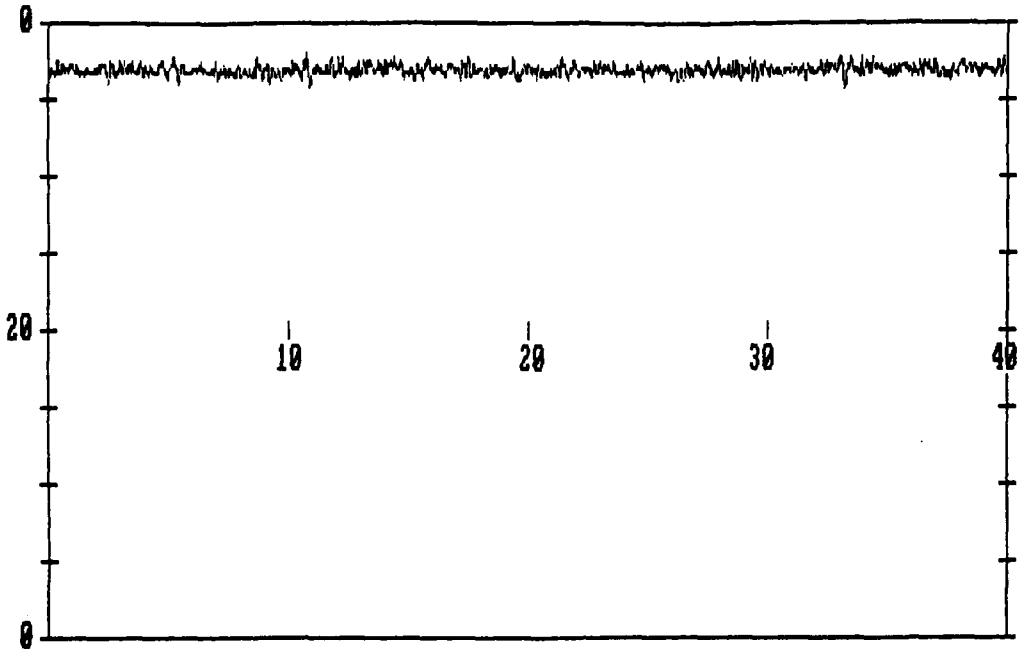

Fig. B-1. Acceptable LSD Measurement

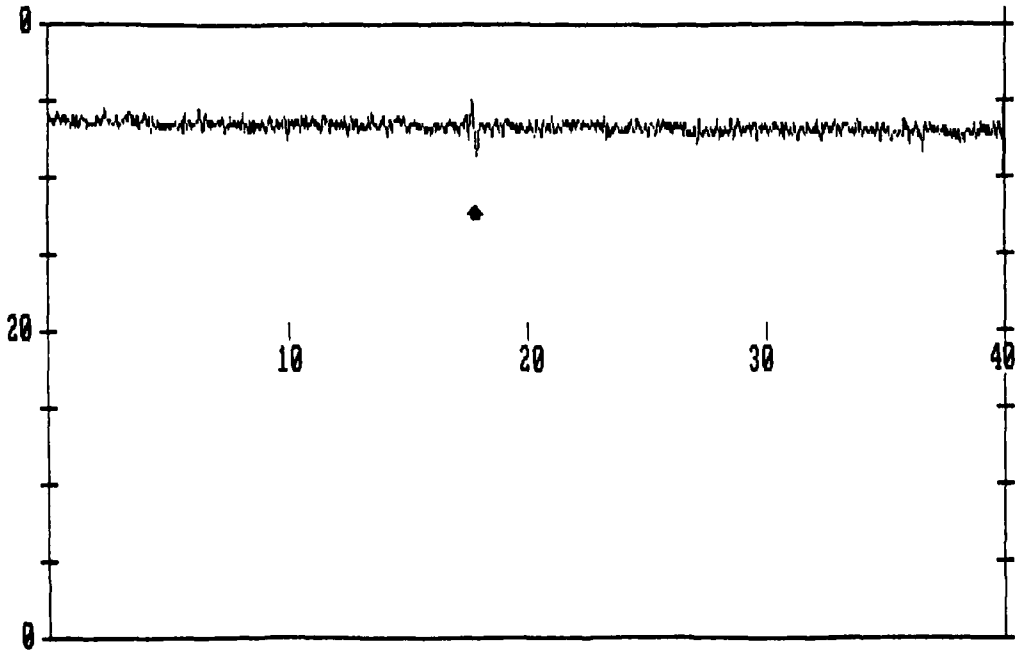

Fig. B-2. LSD Measurement Displaying Metal Damage

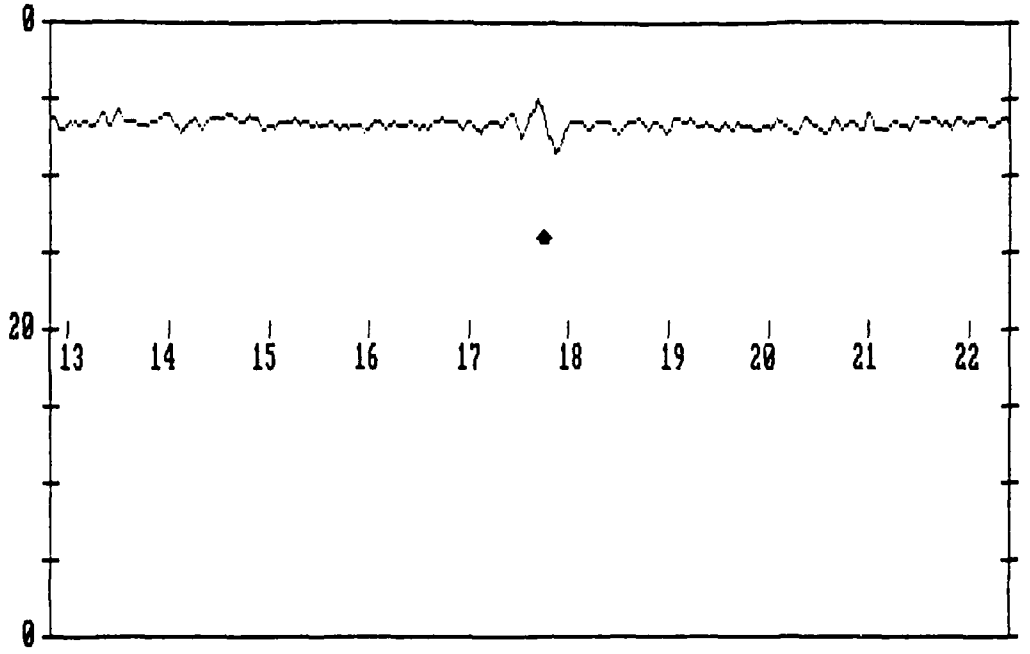

Fig. B-3. Metal Damage Artifact

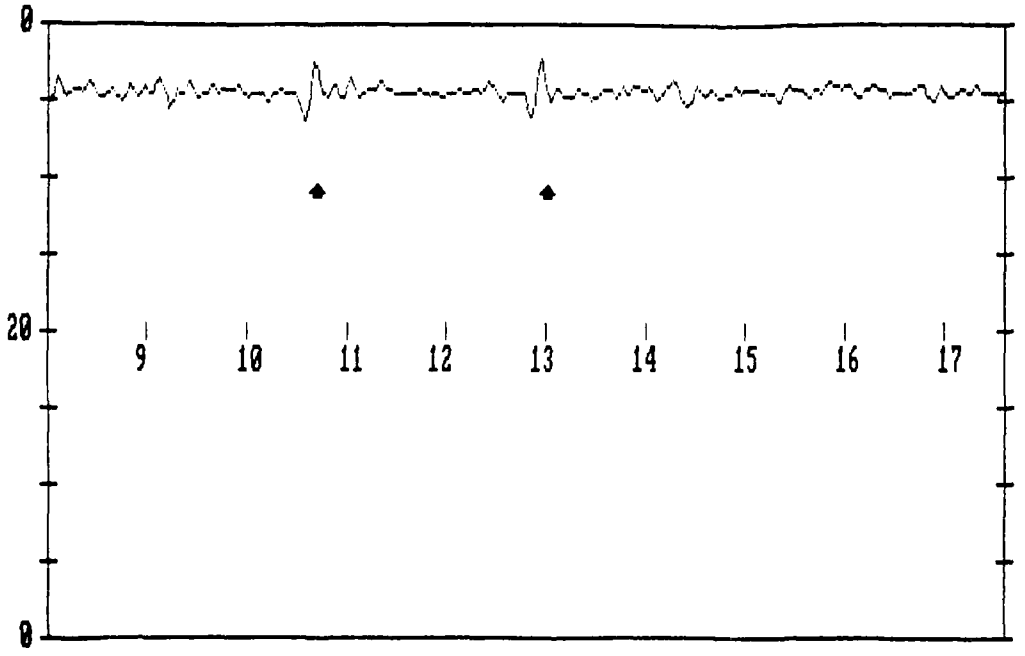

Fig. B-4. Particulate Contamination Artifacts

The random variable w(t) represents the noise in an acceptable measurement as shown in Figure B-1 and v(t) represents the changes in torque created by balls rolling over particles or damaged metal. If the bearing is acceptable, then v(t) = 0 for all t.

The LSD measurements are sampled with period T such that

$$z(k) = z(kT) = w(k) + v(k) \tag{B-3}$$

If the sampling period, T, is small enough so that

$$\lambda T << 1 \tag{B-4}$$

where λ is the Poisson parameter (average density of impulses) then the Poisson probability function [46] given by

$$p_n(t) = Pr\{n \text{ events in time period } t\} = \frac{(\lambda t)^n}{n!} e^{-\lambda t} \tag{B-5}$$

can be stated approximately as

$$\begin{aligned} p_0(T) &\simeq 1 - \lambda T \\ p_1(T) &\simeq \lambda T \\ p_n(T) &\simeq 0 \qquad n>1 \end{aligned} \tag{B-6}$$

This means that the probability of an impulse at any time step is λT;

$$Pr\{v(k) = 0\} = 1 - \lambda T \tag{B-7a}$$

$$Pr\{v(k) \neq 0\} = \lambda T \tag{B-7b}$$

A PDF for the random variable v(k) may be written as follows;

$$p_v(x) = (1 - \lambda T)\, \delta(x) + \lambda T p_a(x) \tag{B-8}$$

which indicates the finite probability, $1 - \lambda T$, that v(k) is exactly zero.

The PDF of the measurement, z(k), is the convolution (denoted by *) of the PDF's of w(k) and v(k), i.e.

$$\begin{aligned} p_z(x) &= p_w(x) * p_v(x) \\ &= (1 - \lambda T) p_w(x) + \lambda T p_w(x) * p_a(x) \end{aligned} \tag{B-9}$$

Threshold Detector

We shall define two complementary hypotheses:

Hypothesis H_0: $v(k) = 0$
Hypothesis H_1: $v(k) \neq 0$

The decision rule is as follows;

Accept H_0 if $\left|z(k) - \bar{z}\right| \leq \gamma$; accept H_1 if $\left|z(k) - \bar{z}\right| > \gamma$.

Restated, if z(k) varies from its mean value by a difference of γ or greater, then assume that an impulse is present. Two types of errors are possible. An error of the first kind (false alarm) occurs if H_1 is accepted when H_0 is true. An error of the second kind (undetected impulse) occurs if H_0 is accepted when H_1 is true. The conditional probabilities associated with these errors are

$$P_1 = Pr\left\{\left|z(k) - \bar{z}\right| > \gamma \;\middle|\; H_0\right\} = Pr\left\{\left|z(k) - \bar{z}\right| > \gamma \;\middle|\; v(k) = 0\right\} \qquad \text{(B-10)}$$

$$P_2 = Pr\left\{\left|z(k) - \bar{z}\right| \leq \gamma \;\middle|\; H_1\right\} = Pr\left\{\left|z(k) - \bar{z}\right| \leq \gamma \;\middle|\; v(k) \neq 0\right\} \qquad \text{(B-11)}$$

These error probabilities can be expressed as:

$$P_1 = 1 - \int_{\bar{z} - \gamma}^{\bar{z} + \gamma} p_w(x)dx \qquad \text{(B-12)}$$

$$P_2 = \int_{\bar{z} - \gamma}^{\bar{z} + \gamma} p_w(x) * p_a(x)dx \qquad \text{(B-13)}$$

If costs Q_1 and Q_2 are associated with errors of the first and second kinds, respectively, than an optimal threshold value, γ, can be found by minimizing the expected loss function;

$$J = Q_1 P_1 + Q_2 P_2 \qquad \text{(B-14)}$$

The probability that the measurement z(k) exceeds the threshold values can be found using equations (B-9), (B-12), and (B-13) to be

$$P = 1 - (1 - \lambda T)(1 - P_1) - \lambda T P_2 \tag{B-15}$$

Special Case - Gaussian PDF's

If w(k) and a_j have the following probability densities;

$$p_w(x) = \frac{1}{2\pi\ \sigma_w} e^{-(x - \overline{w})^2/2\sigma_w^2} \tag{B-16}$$

$$p_a(x) = \frac{1}{2\pi\ \sigma_a} e^{-(x - \overline{a})^2/2\sigma_a^2} \tag{B-17}$$

and if (because $\lambda T << 1$)

$$\overline{z} \approx \overline{w} \tag{B-18}$$

then the error probabilities may be written

$$P_1 = 1 - \int_{-\gamma}^{\gamma} \frac{1}{2\pi\ \sigma_w} e^{-x^2/2\sigma_w^2} dx$$

$$= 1 - F\frac{\gamma}{\sigma_w} + F\frac{-\gamma}{\sigma_w} \tag{B-19}$$

$$P_2 = \int_{-\gamma - \overline{a}}^{\gamma - \overline{a}} \frac{1}{2\pi(\sigma_w^2 + \sigma_a^2)} e^{-x^2/2(\sigma_w^2\ \sigma_a^2)} dx$$

$$= F\left(\frac{\gamma - \bar{a}}{\sigma_w^2 + \sigma_a^2}\right) - F\left(\frac{-\gamma - \bar{a}}{\sigma_w^2 + \sigma_a^2}\right) \qquad \text{(B-20)}$$

where F(x) is the probability integral

$$F(x) = \int_{-\infty}^{x} \frac{1}{2\pi} e^{-u^2/2}\, du. \qquad \text{(B-21)}$$

For the variances;

$$\sigma_w^2 = \sigma_a^2 = \sigma^2$$

and for several values of γ and $\bar{a}$, the error probabilities are given in Table B-I. *These examples illustrate, as might be expected,* that the technique can be made most effective as the ratio $\bar{a}/\sigma$ becomes large.

Filtering of Correlated Measurements

In the foregoing development, no assumptions about the random variable, w(k), other than knowledge of its a priori PDF have been required. We have not required that w(k) be uncorrelated. If w(k) is correlated, then lower error probabilities could be achieved by taking advantage of the correlation. One possible method would be to use a linear predictor as a whitening filter to remove the correlation of the noise, w(k), which masks the sought feature, v(k). This is illustrated in Figure B-5. We assume that w(k) can be represented as an autoregressive (AR) process [44];

$$w(k) = -\sum_{j=1}^{p} c_j w(k-j) + n(k) \qquad \text{(B-22)}$$

where c_j are the AR coefficients and
n(k) is uncorrelated noise with zero mean.

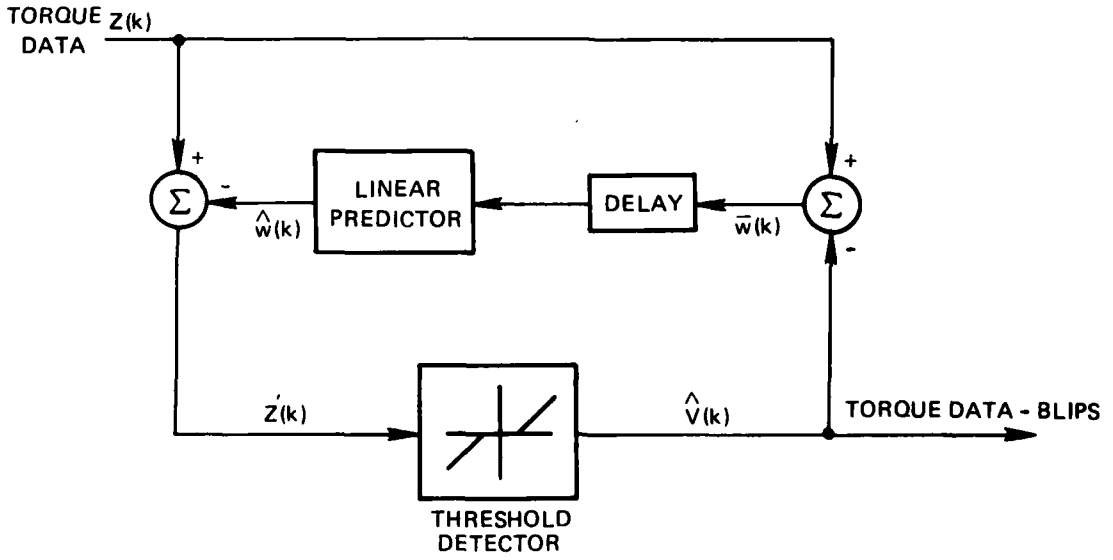

Fig. B-5. Impulse Detector Incorporating Whitening Filter

$\frac{\gamma}{\sigma}$ $\frac{a}{\sigma}$	3	4	6
1	$P_1 = .317$	$P_1 = .317$	$P_1 = .317$
	$P_2 = .077$	$P_2 = .017$	$P_2 = .0002$
2	$P_1 = .046$	$P_1 = .046$	$P_1 = .046$
	$P_2 = .239$	$P_2 = .079$	$P_2 = .002$
3	$P_1 = .003$	$P_1 = .003$	$P_1 = .003$
	$P_2 = .500$	$P_2 = .239$	$P_2 = .017$

TABLE B-I. Error probabilities for special case with Gaussian statistics and $\sigma_w = \sigma_a = \sigma$.

such that w(k) can be predicted using the filter

$$\hat{w}(k) = -\sum_{j=1}^{p} c_j w(k-j) \qquad \text{(B-23)}$$

Using equations (B-3), (B-22), and (B-23), we create the "pseudo-measurement"

$$z'(k) = z(k) - \hat{w}(k) = n(k) + v(k) \qquad \text{(B-24)}$$

and process this using the threshold impulse detector. If an impulse is detected, its estimated intensity, v(k), is subtracted from z(k) for use by the predictor.

If w(k) is correlated, then n(k) will always have smaller variance than w(k) [44] and more reliable detection will result. The PDF of n(k) should be used in place of that for w(k) when calculating error probabilities or optimizing the threshold γ.

APPENDIX C

RESONANCE FREQUENCY OF THE FORCE TRANSDUCER USED IN THE LOW-SPEED DYNAMOMETER

This appendix analyzes the force transducer used to measure bearing drag torque with the low-speed dynamometer. The transducer is a cantilever beam with strain gauges to measure deflection.

The beam used in these tests is 0.745 in. wide, 0.01 in. thick, and has a free length of 1.80 in. It is made of steel.

As shown in Figure C-1, the system is modeled as a beam with one end fixed and the other end attached to a rotational mass with a frictionless joint. The rotational mass consists of the inner race of the bearing and the part of the testing-set-up which leans on the beam (shown in Figure C-2).

To calculate the resonance frequency, we first used a lumped parameter assumption neglecting the mass of the beam, and then checked the result with continuous system dynamics. The results showed that for the size of the bearings of interest the mass of the beam can be assumed negligible, in other words, the first method - which is an approximation - can be used to calculate the resonance frequency.

Using the dimensions of the bearing shown in Figure C-2, the calculated resonance frequency turns out to be:

lumped parameter result: fr = 17.53 Hz

continuous system result: fr = 17.20 Hz

To see the effect of the mass (size) of the bearing on the resonance frequency, resonance frequency is plotted against the bearing mass moment of inertia ranging from 0 to 0.01 lb-in^2 (Figure C-3). (The bearing in Figure C-2 has an inertia of 0.0063 lb-in^2.) As one can see from the plot (Figure C-3), between 0 and 0.003 lb-in^{-2}, the effect of the mass is very strong whereas after 0.006 it becomes quite weak.

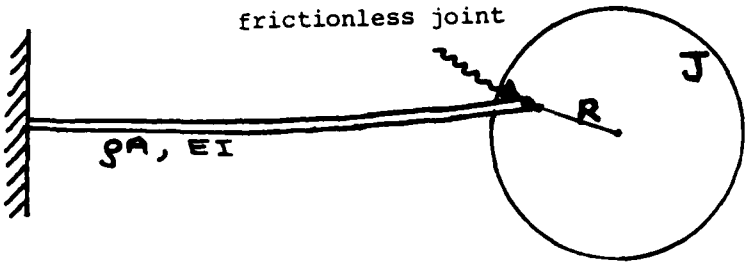

Fig. C-1. System Model

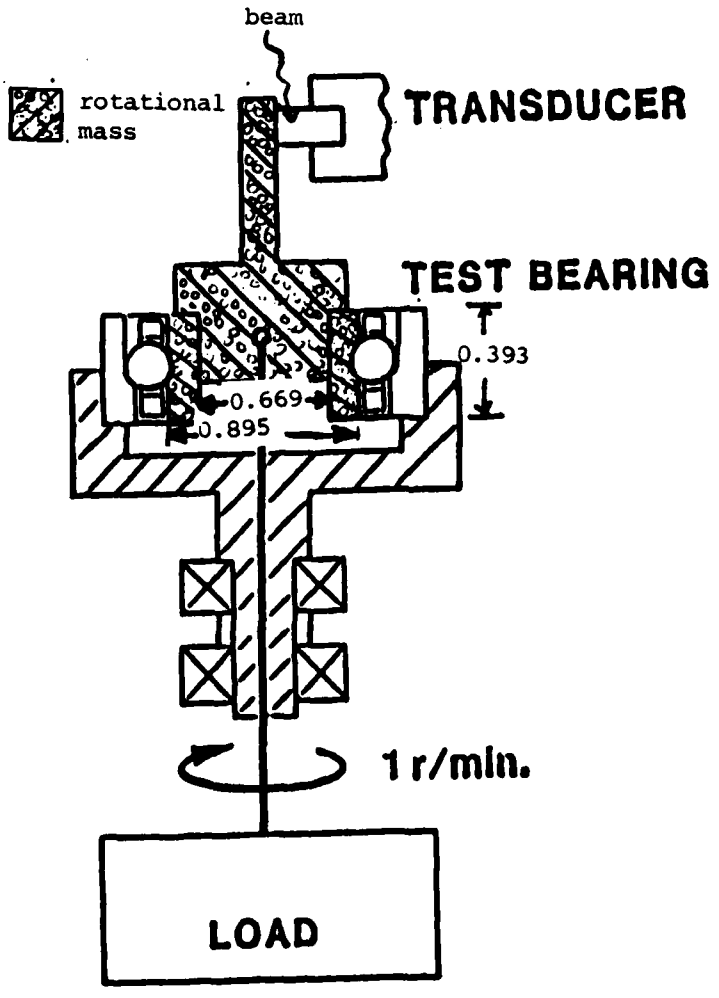

Fig. C-2. Low-Speed Dynamometer

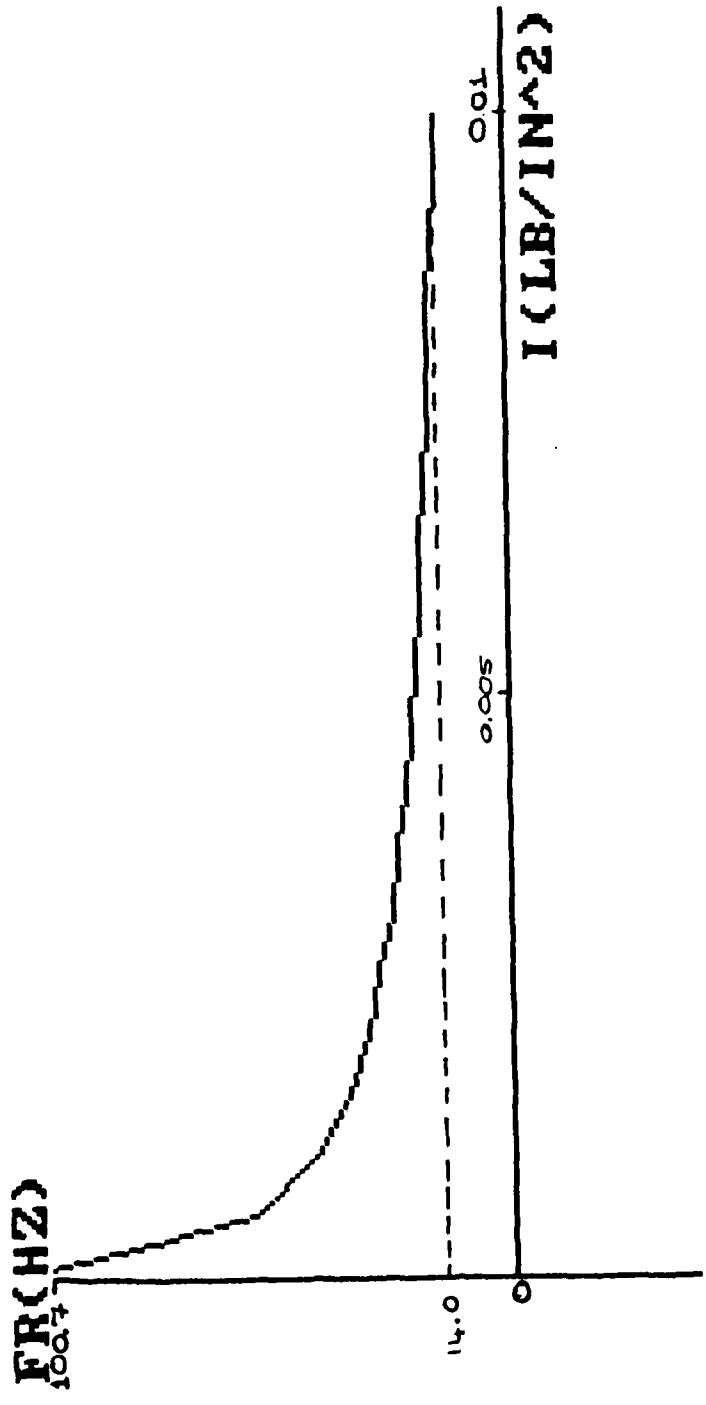

Fig. C-3. Resonance Frequency vs. Mass Moment of Inertia of the Bearing

APPENDIX D

RESULTS OF AUTOMATIC LSD DATA ANALYSIS

LSD data has been processed for 57 individual bearings and bearing pairs. The results are tabulated below. The following defects are tested for:

MT: mean torque exceeds limit
TV: torque variance exceeds limit
MD: metal damage
PC: particulate contamination
UB: unidentified blips
LF: low frequency amplitude exceeds limit
HF: high frequency amplitude exceeds limit
MA: misalignment between bearing pairs

A bearing or bearing pair is considered to fail if one of the following is true:

- mean torque and torque variance too large
- metal damage detected
- more than 3 particulate contamination blips
- misalignment detected
- high or low frequency amplitude exceeds limit

Bearing(s) & Test Number	Pass/Fail	Identified Problems
Individual Bearings		
124 B-1	fail	TV,HF
124 B-2	fail	TV, MD (3), UB, LF, HF
124 B-3	fail	TV, MD (3), UB, LF, HF
129 B-1	fail	TV
129 B-2	fail	MT, TV
130 B-1	fail	MD (1), UB
130 B-2	pass	
131 B-1	pass	
131 B-2	pass	
131 B-3	pass	UB
131 B-4	fail	TV
131 B-5	fail	TV, UB
131 B-6	fail	MT, UB
131 B-7	fail	MT, TV, MD (5), PC (2), UB
134-1	pass	
134-2	pass	

138 B-1	fail	MD (2), UB
138 B-2	pass	UB
142 B-1	fail	MT, TV, UB
142 B-2	fail	TV, MD (1), UB
142 B-3	pass	UB
142 B-4	pass	UB
146 B-1	fail	MT
146 B-2	fail	MT, TV, PC (3), UB, LF, HF
146 B-3	fail	MT
146 B-4	pass	PC (1), UB
146 B-5	pass	UB
146 B-6	pass	UB
146 B-7	fail	MD (6), UB
146 B-8	pass	PC (1), UB
146 B-9	fail	MD (7), UB
146 B-10	fail	UB
146 B-11	pass	UB
146 B-12	pass	UB
146 B-13	fail	MD (1), UB
147 B-1	pass	MD (3), UB
147 B-2	pass	UB
147 B-3	fail	MD (1), UB

Bearing Pairs

117 B-120 B-1	fail	TV, UB, LF
117 B-120 B-2	pass	UB
124 B-130 B-1	pass	
124 B-130 B-3	fail	MD (4), PC (1), UB
124 B-130 B-3	pass	UB
124 B-130 B-4	pass	
124 B-130 B-5	fail	MD (1), PC (2)
124 B-130 B-6	pass	
124 B-130 B-7	pass	
124 B-130 B-8	pass	
124 B-130 B-9	fail	MD (1), UB
124 B-130 B-10	fail	TV, PC (1), UB
124 B-130 B-11	pass	UB, LF, HF
129 B-131 B-1	fail	TV, LF, HF
129 B-131 B-2	fail	TV
134 B-138 B-1	pass	
134 B-138 B-2	pass	PC (1)
141 B-142 B-1	pass	
141 B-142 B-2	fail	TV, MD (1), UB

END

FILMED

3-86

DTIC